© 2022. Published by The Company of Biologists Ltd | Development (2022) 149, dev200701. doi:10.1242/dev.200701

RESEARCH ARTICLE

Formation and function of a highly specialised type of organelle in cardiac valve cells

Christian Meyer[1], Leonhard Breitsprecher[1,2], Laetitia Bataille[3,*], Alain J. M. Vincent[3], Maik Drechsler[1], Heiko Meyer[1,2] and Achim Paululat[1,2,‡]

ABSTRACT

Within a cell, vesicles play a crucial role in the transport of membrane material and proteins to a given target membrane, and thus regulate a variety of cellular functions. Vesicular transport occurs by means of, among others, endocytosis, where cargoes are taken up by the cell and are processed further upon vesicular trafficking, i.e. transported back to the plasma membrane via recycling endosomes or the degraded by fusion of the vesicles with lysosomes. During evolution, a variety of vesicles with individual functions arose, with some of them building up highly specialised subcellular compartments. In this study, we have analysed the biosynthesis of a new vesicular compartment present in the valve cells of *Drosophila melanogaster*. We show that the compartment is formed by invaginations of the plasma membrane and grows via re-routing of the recycling endosomal pathway. This is achieved by inactivation of other membrane-consuming pathways and a plasma membrane-like molecular signature of the compartment in these highly specialised heart cells.

KEY WORDS: Cardiac system, *Drosophila*, Endosomes, GEF, Heart, Inositides, Lysosome, Membrane invagination, Rab5, Rab11, TEM tomography, Tubulation

INTRODUCTION

Cellular compartmentalisation relies, to a considerable extent, on the presence of membrane-enclosed organelles. Each cell continuously generates such compartments of numerous different types, which are required for a wide array of cellular functions. For example, endosomes account for the uptake of extracellular substances, lysosomes for hydrolytic degradation or peroxisomes for initial oxidative degradation. In addition, vesicles also play a crucial role in the transport of membrane components and soluble molecules, i.e. cargoes. Trafficking vesicles continually bud off from one membrane and fuse to another. In metazoans, additional sets of specialised intracellular luminal compartments exist, developed as evolutionary novelties to adapt to specific cellular functions. For example, the T-tubule system of muscle cells permits rapid transmission of action potentials and is crucial to the regulation of the cytoplasmic calcium concentration, which in turn controls myogenic contraction (Setterberg et al., 2021). Melanosomes, another highly specialised organelle, are responsible for the synthesis and storage of melanin pigments in cells (Lin and Fisher, 2007). A further example is the acrosome in spermatozoa of all metazoans, a giant lysosome formed by the Golgi apparatus (Khawar et al., 2019). It contains various enzymes that, once released via exocytosis, penetrate the ECM of the oocyte and pave the way for the sperm.

In this work, we have analysed the origin and biosynthesis of a yet uncharacterised membrane compartment present in valve cells of the *Drosophila* heart. These giant organelles fill most of the cell volume and allow the cells to oscillate between a flattened-elongated and a spherical shape during each heartbeat. The transition between the two states is driven by the contraction and relaxation of intersecting myofilaments. Upon contraction, the cardiac lumen opens and haemolymph flows out of the ventricle into the anterior region of the heart tube. At this point, the membrane compartment ensures elastic deformability of the valve cells, thus facilitating their essential role in regulating the direction of the blood flow within the heart tube. The function of the valve cells has been described in detail previously (Lammers et al., 2017).

Based on a three-dimensional TEM-based reconstruction of cardiac valve cells, we now show that the large valvosomes display remains of pore-like openings towards the plasma membrane. The pores are filled/sealed with electron-dense ECM material. Interestingly, our analysis furthermore revealed that the valvosome membrane constitutes a direct continuation of the plasma membrane, indicating that this novel organelle primarily arises from membrane tubulation events. However, we also found evidence that the formation and maintenance of valvosomes depends on endocytic and membrane recycling pathways. Using RNAi-mediated knockdown, we found that correct endocytosis appears to be crucial for the formation of the valvosomes. Knockdown of Rab5, which is the key GTPase that drives formation of early endosomes (EE) and forwards those EEs to the endosomal maturation pathway (Langemeyer et al., 2018), resulted in complete inhibition of valvosome formation. Downstream endosomal pathways, such as the Rab7-dependent maturation of early endosomes into late endosomes (LE)/multi-vesicular-bodies (MVBs), did not affect valvosome formation. Interestingly, RNAi-mediated downregulation of *rab11* caused a complete inhibition of valvosome formation, indicating an essential role of the endosomal recycling pathway in the assembly of these organelles.

Based on these data, we postulate a model in which the recycling endosome (RE) is recruited to establish and to maintain the valvosome compartment. Our hypothesis is supported by finding

[1]University of Osnabrück, Department of Biology and Chemistry, Zoology and Developmental Biology, Barbarastraße 11, 49076 Osnabrück, Germany. [2]Center of Cellular Nanoanalytics (CellNanOs), integrated Bioimaging Facility (iBiOs), University of Osnabrück, Barbarastrasse 11, 49076 Osnabrück, Germany. [3]Unité de Biologie Moléculaire et Cellulaire et du Développement (MCD), Centre de Biologie Intégrative (CBI), Université de Toulouse UMR 5077/CNRS, F-31062 Toulouse, France.
*Present address: Université Rennes, CNRS, INSERM, IGDR (Institut de Génétique et Développement de Rennes) UMR 6290, ERL U1305, F-35043 Rennes, France.

‡Author for correspondence (achim.paululat@uos.de)

C.M., 0000-0001-8303-5636; L.B., 0000-0001-9880-5939; L.B., 0000-0002-3897-9520; A.J.M.V., 0000-0002-2769-7501; M.D., 0000-0001-7484-6365; A.P., 0000-0002-8845-6859

Handling Editor: Thomas Lecuit
Received 3 March 2022; Accepted 23 August 2022

Development (2022) 149, dev200701. doi:10.1242/dev.200701

that the membrane of this compartment displays a PIP2-PIP3 phosphoinositide signature highly similar to that of the plasma membrane. We further postulate that the valvosome membrane is recognised as a target membrane by REs. Additionally, we found that several membrane-trafficking pathways appear to be inactive in valve cells. We suggest that this evolved to block unnecessary membrane consumption, thus providing sufficient membrane resources for valvosome formation and maintenance.

In summary, we identified well-known vesicular trafficking pathways as being involved in the formation of a yet largely uncharacterised organelle: the valvosome. Valvosomes primarily arise from membrane invagination events, but mature and are maintained by recycling endosomes that fuse with it. We postulate an entirely new cell biological mechanism, in which several Rab-dependent pathways are turned off to increase the availability of membrane material required for valvosome maintenance. From a physiological point of view, it is crucial for the valve cell to ensure lifetime maintenance of the valvosome, as there is no repair mechanism or any renewal from stem cells known in the *Drosophila* heart.

RESULTS

The larval *Drosophila* heart constitutes a simple muscular pump that directs the flow of haemolymph through the body cavity. Flow direction is significantly impacted by one pair of valve cells that separate the linear organ into an anterior aorta and a posterior heart chamber (Fig. 1). Valve cells are determined during embryogenesis, and arise from embryonic cardioblasts, while they further differentiate throughout larval development as integral constituents of the heart tube (Lammers et al., 2017; Lehmacher et al., 2012, 2009). At late larval stages, valve cells typically contain two to four giant membrane-enclosed compartments, which we named valvosomes (Fig. 1, asterisks). Valvosomes allow the valve cells to undergo dynamic cell shape changes during heart contraction, which result in a periodic closing and opening of the heart lumen (Fig. S1). In the present study, we investigated how valvosomes are formed and maintained, with a special focus on identifying membrane-trafficking pathways that are crucial to these processes.

Valvosome membranes are negative for classical endomembrane markers

In a previous study, we provided evidence that the small GTPase Rab5 plays a key role in valvosome formation, indicating that Rab5-mediated endocytosis is vital for the biogenesis of these membrane compartments (Lammers et al., 2017). However, the origin and identity of valvosome membranes was not clear thus far. To test, whether valvosomes constitute specialised endomembranes, we started to systematically analyse the subcellular localisation of various organelle markers in valve cells. Although vital for valvosome formation, we found that Rab5 predominantly localised in a dotted pattern around the nucleus and in the cytoplasm, but was absent from valvosomal membranes (Fig. 1D). Rab5-positive endocytic vesicles transport internalised receptors and membrane proteins to recycling endosomes, which are decorated by the small GTPase Rab11. Recycling endosomes will then transport cargoes back to the plasma membrane. As knockdown of *rab5* impacted valvosome formation (Lammers et al., 2017), but the protein itself appeared not to be associated with valvosome membranes, we next investigated the localisation of the GTPase Rab11. Similar to Rab5, Rab11 was distributed in a spotted pattern around the nucleus and smaller cytoplasmic parts of the cell, but did not decorate the valvosome membrane (Fig. 1E). Endosomal vesicles are known to grow by membrane fusion (Spang, 2016). Therefore, we considered it possible that valvosomes might represent other endosomal compartments, like enlarged late endosomes (LE), multivesicular bodies (MVB) or lysosomes. Consequently, we stained cells for the GTPase Rab7 and for Lysosome-associated membrane protein 1 (Lamp1), which are established membrane markers for the MVB/LE/lysosomal compartments. In valve cells, Rab7 and Lamp1 both localised in a punctate pattern (Fig. 1F,G). Signals associated with smaller vesicular structures were distributed randomly throughout the cytoplasm of the cells. Neither Rab7 nor Lamp1 was observed at the membrane of valvosomes (Fig. 1F,G). In line with this observation, we detected no acidification of valvosomes when cells were labelled with Lysotracker. Lysotracker-positive signals were rather restricted to vesicles homogeneously distributed throughout the cytoplasm (Fig. 1H). This observation argued against the hypothesis that valvosomes are enlarged LE/MVBs or lysosomal derivatives. Another major endosomal route within a cell is the maturation of early endosomes into autophagosomes (Gatica et al., 2018). To test whether valvosomes constitute autophagosomal derivatives, we stained cells for the autophagosome-specific ubiquitin-like protein Atg8 (Fig. 1I). Although a few Atg8-positive dotted structures were homogeneously distributed throughout the cytoplasm, valvosome membranes did not exhibit any Atg8-positive signals (Fig. 1I). Finally, markers for the Golgi apparatus (EYFP-tagged Golgi localisation sequence of the human type 1 γ-glutamyltransferase) or the endoplasmic reticulum (ER)-resident chaperone Calnexin did also not colocalise with valvosome membranes (Fig. 1J,K) (LaJeunesse et al., 2004).

In summary, our findings indicate that valvosomes are neither enlarged late endosomes nor multivesicular bodies (MVBs), lysosomes, autophagosomes or any other classical endomembranous organelle. However, we could demonstrate that Rab5 is necessary for valvosome formation (Lammers et al., 2017), indicating that Rab5-mediated endocytosis is involved in this process.

Valvosome growth and maintenance depend on the small GTPase Rab11

RNAi-mediated knockdown of *rab5* by the heart-specific driver *hand*C-Gal4 results in valve cells that completely lack valvosomes (Lammers et al., 2017). To gain a more detailed understanding of this observation, we measured the size and abundance of valvosomes in single wild-type and *rab5* knockdown cells. We confirmed the previously described phenotype, and found that Rab5-depleted cells displayed a reduced number and size of valvosomes, compared with wild type. In addition, the overall size of the cells was decreased (Fig. 2B-B″,H-L). To substantiate our findings, we verified this result by using a second RNAi hairpin directed against *rab5*, which resulted in a similar phenotype to that shown before (Fig. S2). In order to exclude secondary effects from other cells and tissues, we repeated the *rab5* knockdown, using a *toll*-Gal4 driver line (Sellin et al., 2006). The *toll*-Gal4 driver is expressed in all embryonic cardioblasts, but becomes valve cell exclusive during larval stages, when valve cells start to differentiate. As observed for the *hand*-Gal4-driven knockdown, *toll>rab5* RNAi valve cells exhibit a smaller cell size, fewer valvosomes per cell as well as smaller valvosomes (Fig. 2C-C″,H-J). In our hands, the effect seems to be even stronger when *toll*-Gal4 was used as driver line. Although not tested, this might be due to different expression levels in valve cells of both drivers used. However, in conclusion this demonstrates that Rab5 is crucial for proper valvosome formation in a cell-autonomous manner.

Development (2022) 149, dev200701. doi:10.1242/dev.200701

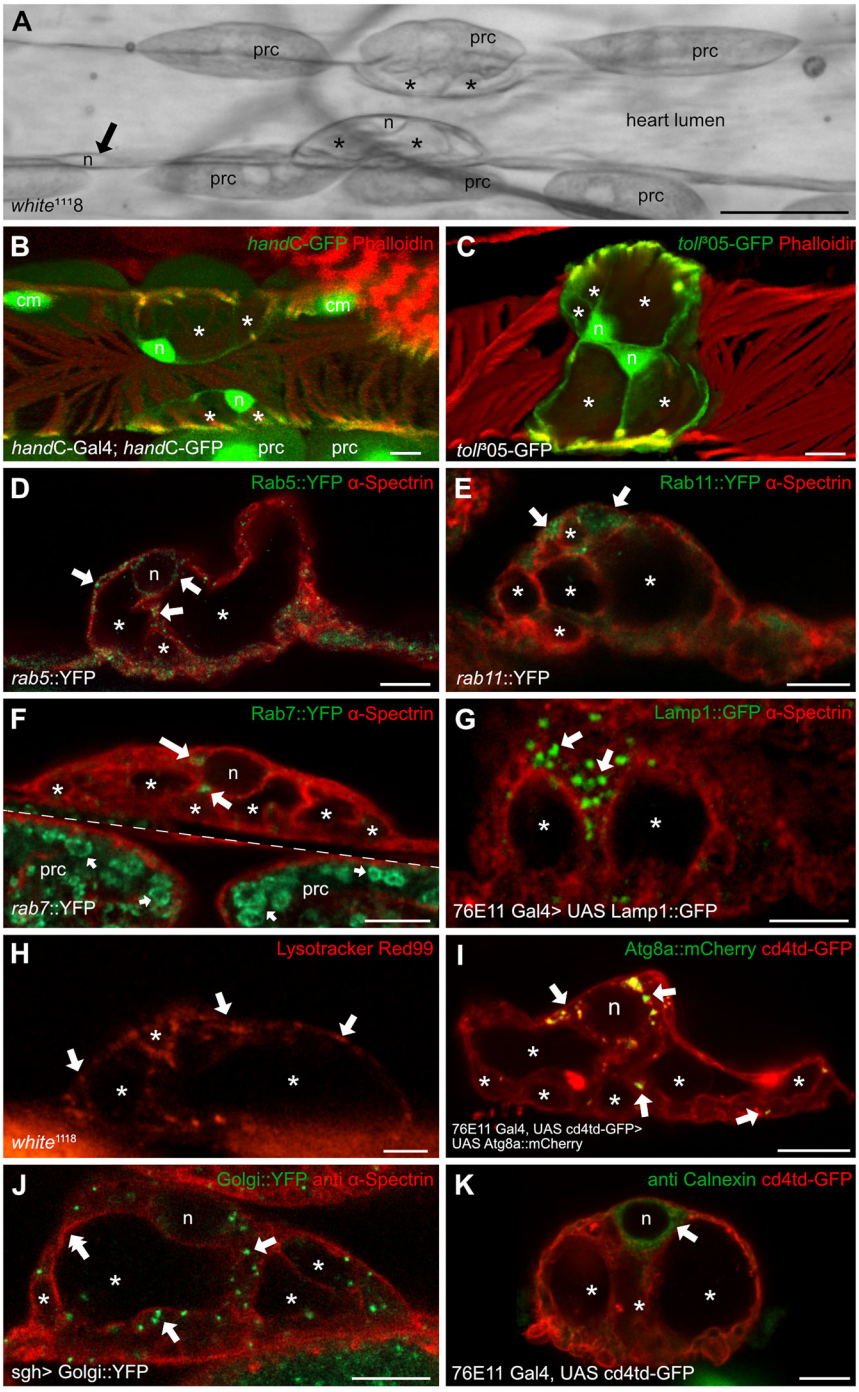

Fig. 1. Valvosomes represent a new type of organelle. (A) Bright-field image of a 3rd instar larval heart tube. Valve cells are distinguishable from other cardiomyocytes (arrow) by their cell shape and the large intracellular organelles. Nuclei (n) are labelled. Scale bar: 50 µm. (B,C) Valve cells at the elongated 'open' state (B) and at the spheric 'closed' state (C). Pericardial cells (prc) and cardiomyocytes (cm), including the valve cells, are labelled with *hand*C>GFP (green channel) or valves only with *toll*>GFP; all muscles are stained for phalloidin (red channel). (D) Rab5 (green channel) labels early endosomes in the cytoplasm (arrows) but not the valvosome. (E) Rab11 (green channel) labels recycling endosomes in the cytoplasm (arrows) of the cells but not the valvosomes. (F) Rab7 (green channel) labels late endosomes (arrows) in the cytoplasm but not the valvosomes. Adjacent pericardial nephrocytes exhibit many Rab7-positive vesicles (smaller arrows). (G) Lamp1 (green channel) associates with lysosomes within the cytoplasm of the cell (arrows) but not with the valvosomes. (H) The luminal content of the valvosome is not acidified, as revealed by Lysotracker staining (arrows). (I) Autophagosomes are decorated with Atg8a (green channel) and are present in the cytoplasm (arrows). (J) Secretory vesicles are visualised by expression of a GFP-tagged Golgi targeting sequence (green channel) and found solely in the cytoplasm and in close proximity to the valvosomal membrane (arrows). (K) Calnexin (green channel) marks the endoplasmic reticulum and shows a strong signal around the nucleus (arrow) but not on the valvosome membrane. As a counterstain (red channel), Spectrin (D-G,J) or membrane-bound GFP (I,K) were used. Scale bars: 10 µm. Valvosomes are labelled with asterisks.

We next knocked down expression of *rab7* in all heart cells (*hand*C-Gal4), including valve cells, conventional cardiomyocytes and pericardial nephrocytes, using two independent hairpins (Fig. S2). The nephrocytes served as an internal *in vivo* control for knockdown efficiency. Analyses by light- and electron microscopy revealed that Rab7-depleted pericardial cells showed morphological differences compared with wild type, indicating that the knock-down was effective (data not shown). However, *rab7*-depleted valve cells exhibited valvosomes that were comparable in size and number to wild type (Fig. 2D-D″,H-J). Thus, knockdown of *rab7* and therefore the maturation of later endosomal derivatives seems not necessary to form valvosomes. Thus, we next tested whether proteins involved in the formation and function of recycling endosomes might be involved. Cells use two major recycling pathways: one depending on the small GTPase Rab4 (fast recycling) and one on the GTPase Rab11 (slow recycling) (Grosshans et al., 2006; Maxfield and McGraw, 2004; Sheff et al., 1999; Ullrich et al., 1996; Zerial and McBride, 2001). To test whether either of those proteins is expressed in valve cells, we analysed the expression of Rab4 and Rab11, using gene-specific Gal4 driver lines (Chan et al., 2011). When crossed to a UAS-GFP transgene, we only found Rab11 to be expressed in valve cells, while Rab4 was absent (see below). Thus, we excluded a major role for Rab4 in valvosome formation.

RNAi-mediated downregulation of *rab11*, by two independent hairpins, resulted in a dramatic effect on the differentiation of valve

Development (2022) 149, dev200701. doi:10.1242/dev.200701

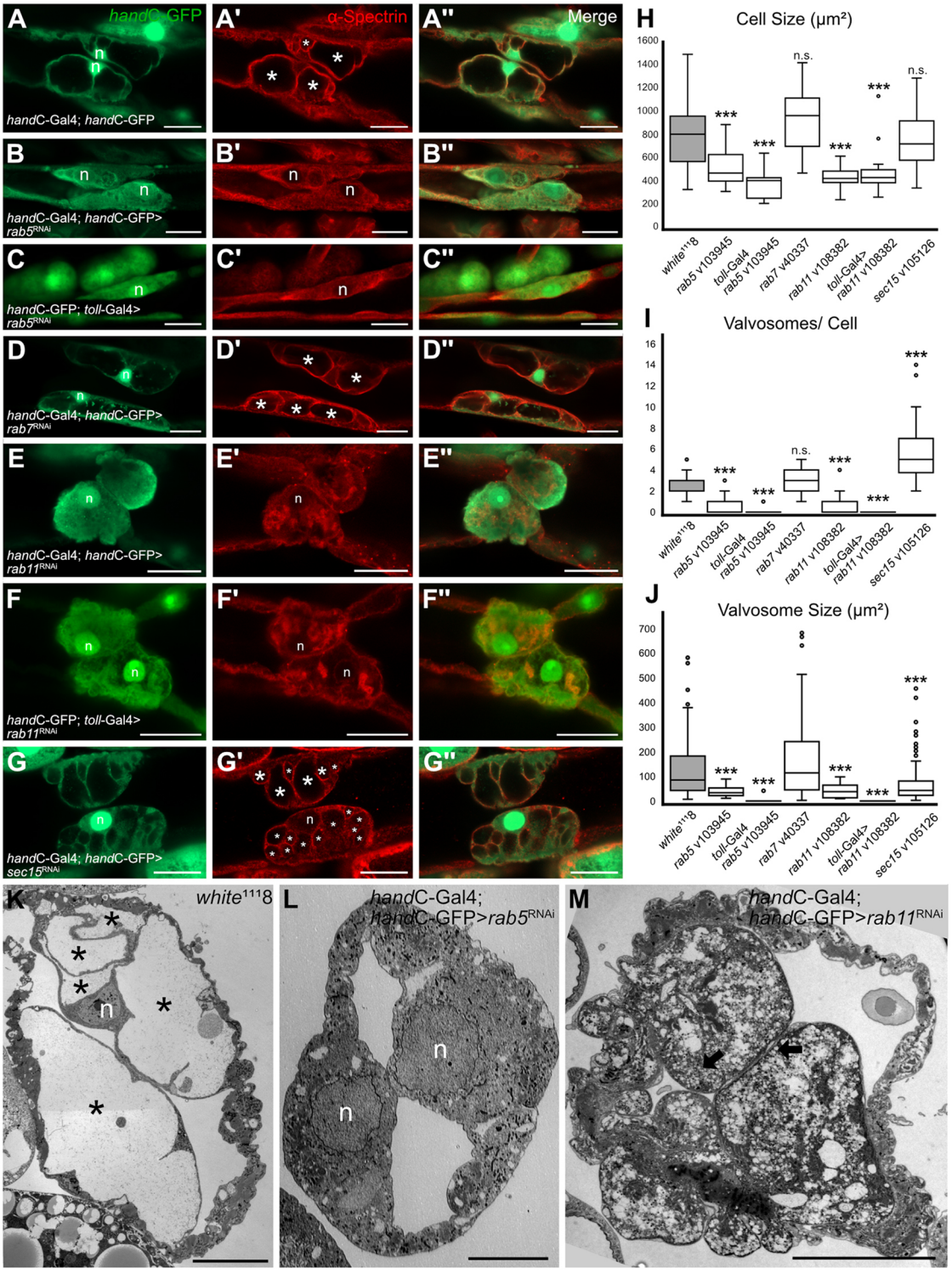

Fig. 2. Valvosomal growth and maintenance depend on the endosomal recycling pathway. (A-A″) In control flies, the valvosome compartment (asterisks) is properly made and labelled by Spectrin staining. (B-D″) Knockdown of *rab5* inhibits valvosome formation (B-C″), whereas knockdown of *rab7* has no effect on valvosome differentiation (asterisks, D-D″). (E-F″) Blocking the recycling endosomal pathway by knockdown of *rab11* results in a complete absence of large valvosomes. (G-G″) Knockdown of the exocyst complex subunit Sec15 leads to an increased number of smaller valvosomes (asterisks). (H-J) Statistical analyses of the *rab5*, *rab7*, *rab11* and *sec15* knockdown effects. RNAi expression was driven by *hand*C-Gal4 if not stated otherwise. Inhibiting endocytosis or the recycling pathway leads to smaller cells, with the total number of valvosomes and their average size being highly reduced. Interfering with the exocyst complex by downregulation of its subunit Sec15 leads to significantly more but smaller valvosomes. Knockdown of *rab7* has no effect on valvosome histology or number. Cells analysed were *white*^{1118} (*n*=38), *rab5* (*n*=40), *toll*-Gal4>*rab5* (*n*=12), *rab7* (*n*=38), *rab11* (*n*=38), *toll*-Gal4>*rab11* (*n*=18) and *sec15* (*n*=38). **P*<0.05, ***P*<0.01, ****P*<0.001; (K-M) Electron microscopic cross-sections of valve cells confirmed absence of valvosomes in *rab5* and *rab11* knockdown animals. Although *rab5* animals show basically no endosomes or other vesicular compartments (L), early endosomes and other vesicles are present in *rab11* knockdown animals (black arrows), yet large valvosomal compartments are absent (M). In control cells, valvosomes are properly formed (K, asterisks). Scale bars: 20 μm in A-G″; 10 μm in K-M. n, nucleus.

Development (2022) 149, dev200701. doi:10.1242/dev.200701

cells and the formation of valvosomes (Fig. 2E-F″,H-J,M). Cells depleted for *rab11* expression were significantly smaller compared with control cells (Fig. 2H). The most prominent phenotype was the nearly complete lack of larger membrane compartments, including valvosomes. Instead, the cells were largely filled with a high number of smaller vesicles. These vesicles were comparable in size with other endosomal carriers (Fig. 2M). Light microscopic analysis, using the cell cortex marker α-Spectrin as a counterstain (Fig. 2E-F″), further revealed that valvosomes were completely absent in Rab11-depeleted cells. In contrast, control cells exhibited a clear α-Spectrin signal outlining the valvosome (Fig. 2A-A″). Absence of valvosomes in response to *rab11* knockdown was confirmed by ultrastructural analyses (TEM) (Fig. 2M). Importantly, one of the RNAi hairpins directed against *rab11* had only mild effects on valve cells. However, the cells did show similar lack of valvosomes and a reduced cell size (Fig. S2). A valve cell-specific knockdown of *rab11* using *toll*-Gal4 had the same effect on valvosome formation (Fig. 2F-F″,H-J). Thus, as shown for *rab5*, the function of *rab11* seems to be cell-autonomous. To further support the idea that membrane recycling and exocytosis are crucial for valvosome formation, we also knocked down the exocyst component Sec15, again using two independent hairpins (Fig. 2G-J). Sec15 constitutes an effector protein of activated Rab11, and forms a key component of the exocyst, by regulating integrity and stability of the complex. In *Drosophila* and mammals, the exocyst complex is recruited to recycling endosomes via interaction of its Sec15 with the C-terminal domain of membrane-localised Rab11 (Wen et al., 2020; Wu et al., 2005; Zhang et al., 2004). The recycling endosome is then tethered to, and fuses with, the plasma membrane, delivering recycled membrane material and proteins. Compared with the knockdown of *rab5* and *rab11*, depletion of *sec15* did not alter the size of valve cells. Downregulation of *sec15* did, however, result in an increased number of valvosomes, while valvosomal size was significantly reduced, similar to the knockdown of *rab5* and *rab11* (Fig. 2H-J). These phenotypes were observed for both hairpins used (Fig. S2). From this we concluded that, in the absence of Sec15, recycling endosomes may fail to tether efficiently to the valvosome membrane, resulting in smaller valvosomes that are unable to fuse and thus grow in size.

In summary, reduction of *rab5* and *rab11* caused a major inhibition of valvosome formation, while the depletion of *sec15* left the formation of valvosomes intact, but interfered with the maturation of the organelle. Together, these results indicate that valvosome formation requires a cell-autonomous, functional Rab5/Rab11-dependent endosomal biogenesis pathway, as well as membrane tethering by the exocyst complex. We postulate that the unique histology of the valve cell potentially evolved by redirecting the canonical Rab11-dependent endosomal recycling pathway into a valvosome-supporting pathway.

Valvosomes exhibit molecular signatures of the plasma membrane

In our working model thus far, the valvosome membranes seem to serve as an acceptor membrane for Rab11-dependent recycling endosomes, similar to the plasma membrane. Thus, we wondered whether valvosome membranes and the plasma membrane share similar biochemical signatures.

The cell cortex marker α-Spectrin lines the intracellular (cytosolic) side of the plasma membrane in all eukaryotic cells. Spectrin forms complex cytoskeletal arrangements that serve as a scaffold to connect to the actin cytoskeleton of the cells. This scaffold is crucial for maintaining the membrane integrity of every cell. We noted that α-Spectrin lines the complete perimeter of the valvosomes (e.g. Fig. 4B,E,H). This distinct localisation is highly similar to the Spectrin pattern beneath the plasma membrane, and thus supports our model that the plasma membrane and valvosomal membranes share a similar molecular signature. Considering the continuous mechanical stress that valve cells are exposed to during each heartbeat, we analysed whether the Spectrin cytoskeleton is

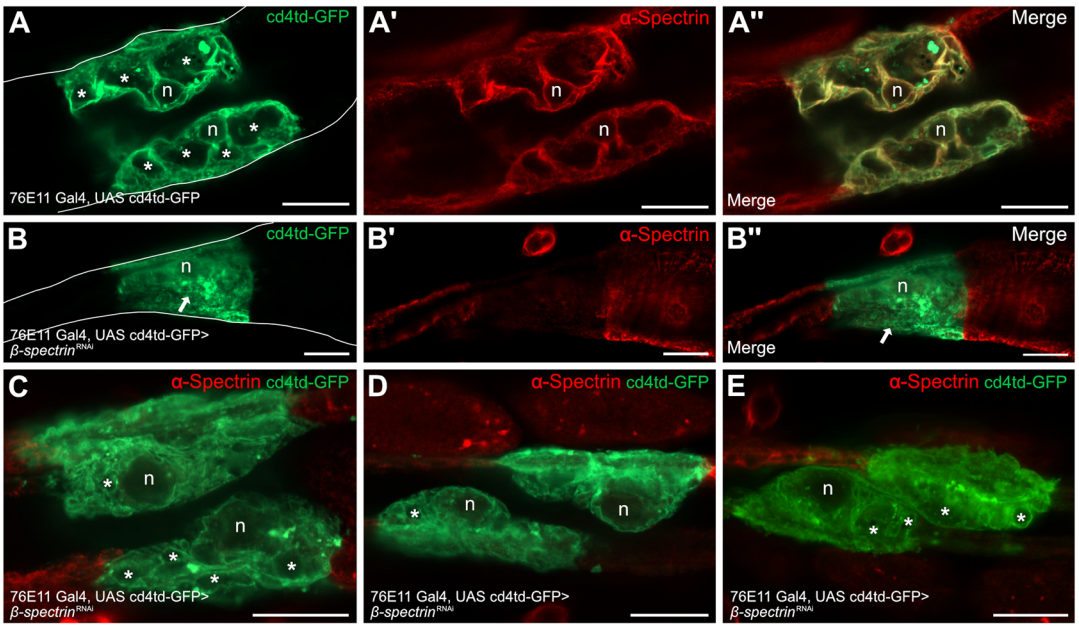

Fig. 3. Spectrin is crucial for proper valve cell histology. (A-A″) In control flies, Spectrin colocalises with membrane-bound GFP (cd4td-GFP) and labels the plasma membrane and the valvosomal membrane. (B-B″) Valve cell-specific knockdown of *spectrin* leads to a reduced Spectrin signal in the valve cells (arrows) and impairs valvosome integrity. (C-E) Upon *spectrin* downregulation, valvosomes are still present but appear collapsed (B-D, spectrin RNAi v42054; E, spectrin RNAi v42053). Scale bars: 20 µm. n, nucleus. Valvosomes are labelled with asterisks.

Development (2022) 149, dev200701. doi:10.1242/dev.200701

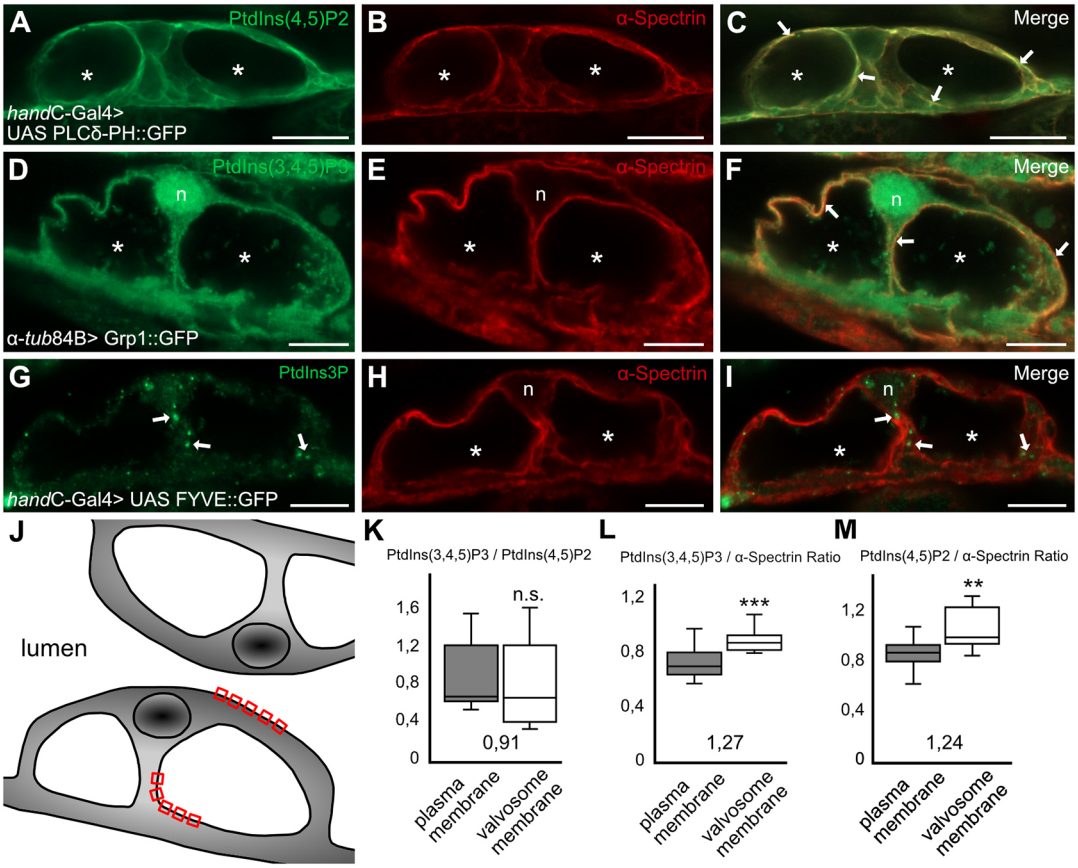

Fig. 4. The membrane of the valvosome exhibits a similar lipid signature to the plasma membrane. (A-C) Valve cells stained for GFP-tagged pleckstrin homology domain from human PLCD to label phosphatidylinositol-4,5-bisphosphate [PtdIns(4,5)P_2]. PtdIns(4,5)P_2 is homogenously distributed within the plasma membrane of the cell but also lines the valvosomal membrane (arrows). Scale bars: 20 µm. (D-F) Analysis of a GFP-tagged pleckstrin homology domain of Grp1 revealed the presence of phosphatidylinositol-3,4,5-trisphosphate [PtdIns(3,4,5)P_3] in the plasma membrane, as well as in the membrane of the valvosome (arrows). Scale bars: 10 µm. (G-I) Phosphatidylinositol-3-phosphate is present on endosomes in the cytoplasm of the cell (arrows), as visualised by expression of a GFP-tagged FYVE zinc-finger domain. Scale bars: 10 µm. (J) The scheme illustrates the points of measurement at the plasma membrane and at the valvosomal membrane, respectively (red boxes). (K-M) The relative ratio of PtdIns(3,4,5)P_3 to PtdIns(4,5)P_2 is identical between the plasma and valvosomal membrane (factor 0.91, K). Relative to the plasma membrane, significantly more PtdIns(3,4,5)P_3 (factor 1,27, L) and PtdIns(4,5)P_2 (factor 1,24, M) are detected in the valvosome membrane. $^{**}P<0.01$, $^{***}P<0.001$.

required for the differentiation and maintenance of the cells. Valve cell-specific knockdown of β-Spectrin transcripts considerably reduced the amount of α-Spectrin protein at the valvosome membrane, as confirmed by antibody staining (Fig. 3B-B″). This indicated that the knockdown of the β subunit was sufficient to inhibit proper formation of the Spectrin cytoskeleton. However, valvosomes are generated in β-Spectrin-depleted cells, but seem to be collapsed, as indicated by the expression of membrane-targeted GFP (Fig. 3C-E). Of note, vertebrate Spectrin represents the main structural component conferring mechanical resistance and deformability to erythrocytes (Skalak and Chien, 1982; Stokke et al., 1986). Interestingly, valve cells failed to form stable valvosomes as a result of β-Spectrin knockdown. However, remnants of the valvosome membrane were still present, which may reflect destabilised and collapsed valvosomes (Fig. 3C-E, asterisks). This scenario would support a function of the Spectrin cytoskeleton in stabilising the valvosomal structure, probably in a similar manner to the maintenance of erythrocyte shape and mechanical stability by vertebrate Spectrin.

The finding that valvosomes are decorated with α-Spectrin (Fig. 3), a cytoskeletal protein usually associated with the plasma membrane, already hinted that the origin of valvosomes might be the plasma membrane. It is a widely accepted concept that membranous organelles of individual cellular trafficking pathways and the plasma membrane exhibit a different, yet characteristic, lipid composition. This lipid signature serves as a cellular zip code and, for example, is necessary to become recognised as an acceptor membrane for specific Rab proteins or tethering factors, and to ensure correct delivery of endosomal cargo. Such specificity is mainly achieved by incorporation of distinct phosphoinositides into the particular membrane. Phosphoinositides (PtdIns) can be phosphorylated to form different varieties of phosphorylated phosphoinositides (called PIPs) that in turn often serve as direct interaction partners of tethering factors or other effector proteins/protein complexes involved in vesicular maturation or turnover. Whereas plasma membranes are typically enriched in PtdIns(4,5)P_2 (PIP2) and PtdIns(3,4,5)P_3 (PIP3), they are low in, for example, PtdIns3P. In contrast, PtdIns3P is typically found in membranes of early endosomes, which in turn lack PIP2 and PIP3 (Volpatti et al., 2019). In order to monitor the distribution of different PIPs in valve cells, we expressed GFP-tagged Pleckstrin-homology domains (PH-domains) of Phospholipase C or Grp1, which bind PIP2 and PIP3, respectively. Both reporter proteins decorated the plasma membrane and the valvosome membrane of the cell, indicating that

Development (2022) 149, dev200701. doi:10.1242/dev.200701

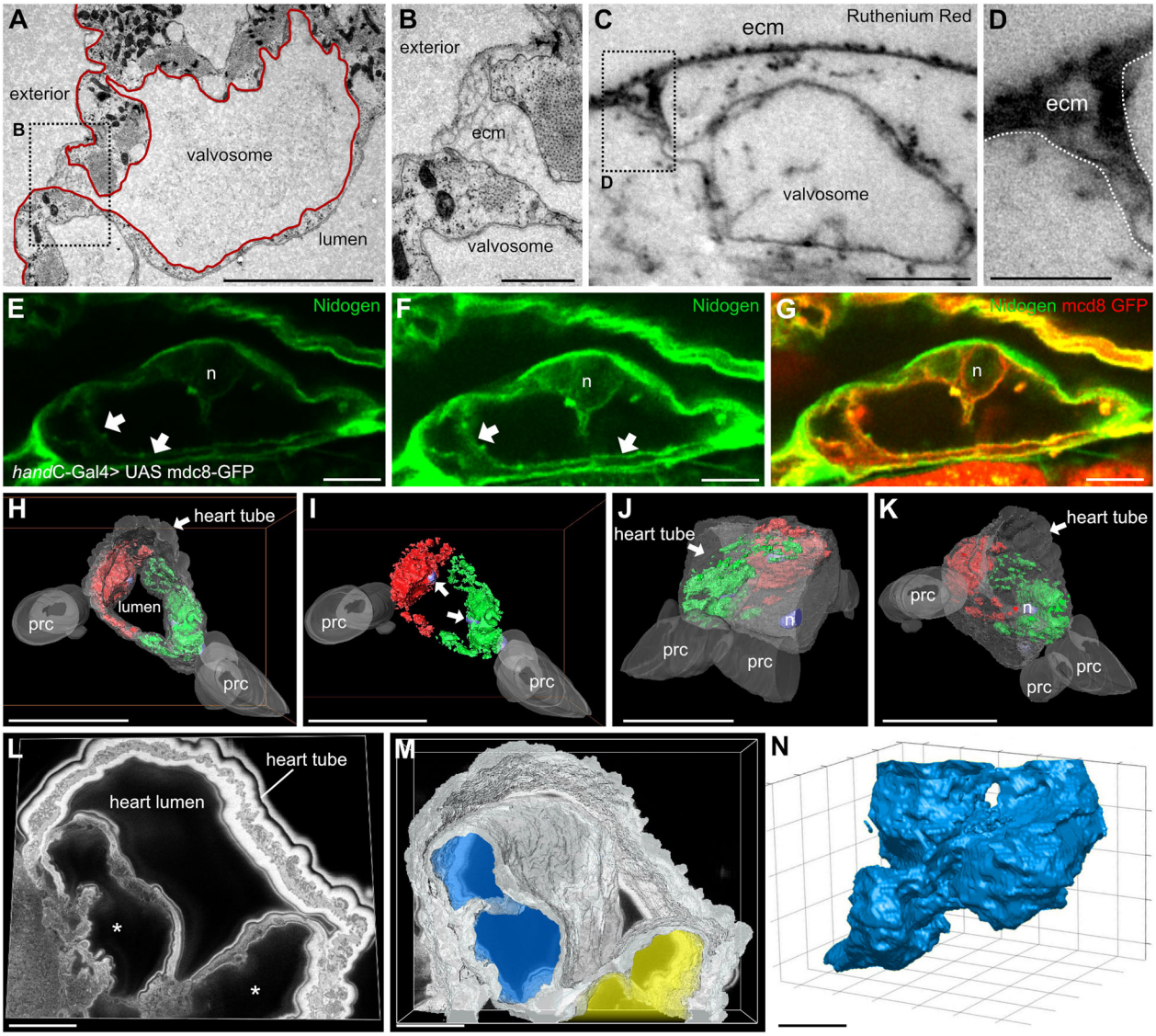

Fig. 5. Valvosomes derive from plasma membrane tubulation and occupy most of the valve cell volume. (A-D) TEM analysis reveals plasma membrane invaginations as a source of valvosome formation. The valvosome membrane is in direct continuity with the plasma membrane (outlined in B and D). (C,D) The invagination pore is filled with extracellular matrix material (ecm) and stained by Ruthenium Red. Scale bars: 5 µm in A,B; 500 nm in C; 250 nm in D. (E-G) Nidogen, a canonical extracellular matrix constituent, is found on the plasma membrane, as well as on the luminal side of the valvosomal membrane (arrows), where it colocalises with membrane-bound GFP (mcd8 GFP; F is an overexposed version of E). Scale bars: 10 µm. (H-K) Three-dimensional model generated from a series of semi-thin sections. The valvosomal compartment (red and green) of each valve cell is shown. Scale bars: 50 µm. (H) Cross-sectional view of the two valve cells in an elongated form reflecting the open state during heartbeat. (I) Cross-sectional view of the valvosomal compartments of valve cells (red and green). The nuclei of each valve cell face the luminal side of the heart (arrows). (J) Lateral view of valvosomal compartments slightly shifted along the longitudinal axis of the heart and nuclei of adjacent cardiomyocyte. (K) Ventral view displaying valvosomal compartments distributed all over the cell. In the analysed area, valvosomal compartments occupy 20% of the cells. (L-N) Serial block face EM analysis reveals the three-dimensional histology of valvosomal sub-compartments. Scale bars: 10 µm. (L) Single slice of sectioned area showing heart tube building up a heart lumen and two valve cells (asterisks). (M) Volume rendered image of the heart tube and the two valve cells coloured sheer white. Valvosomal compartment of the left valve depicted in sheer blue and the right in sheer yellow. (N) Volume rendered image of the valvosomal compartment (blue area from M). In the analysed area, the compartment occupies 65% of the volume of the cell. ecm, extracellular matrix; n, nucleus; prc, pericardial cell. Valvosomes are labelled with asterisks.

both membranes share a similar molecular signature (Fig. 4A-F). In contrast, expression of a FYVE-domain GFP-reporter, specifically binding to PtdIns3P, showed an enrichment of the reporter construct in early endosomes and autophagosomes (Simonsen et al., 1998), but did not localise to the valvosomes or the plasma membrane (Fig. 4G-I). Instead, we found spotted signals randomly distributed throughout the cytoplasm of the valve cells, similar to the signals obtained by staining for other endosomal marker proteins (compare with Fig. 1). This indicated that valvosomes and plasma membrane exhibit a similar PIP code.

To strengthen our argument that the plasma membrane and the valvosomal membranes share a similar molecular signature, we compared the relative amounts of PIP2 and PIP3 in both membranes. When both reporters were compared with each other, we found that the PIP2 to PIP3 ratios in the plasma membrane and in the valvosomal membrane were identical, within the limits of

Development (2022) 149, dev200701. doi:10.1242/dev.200701

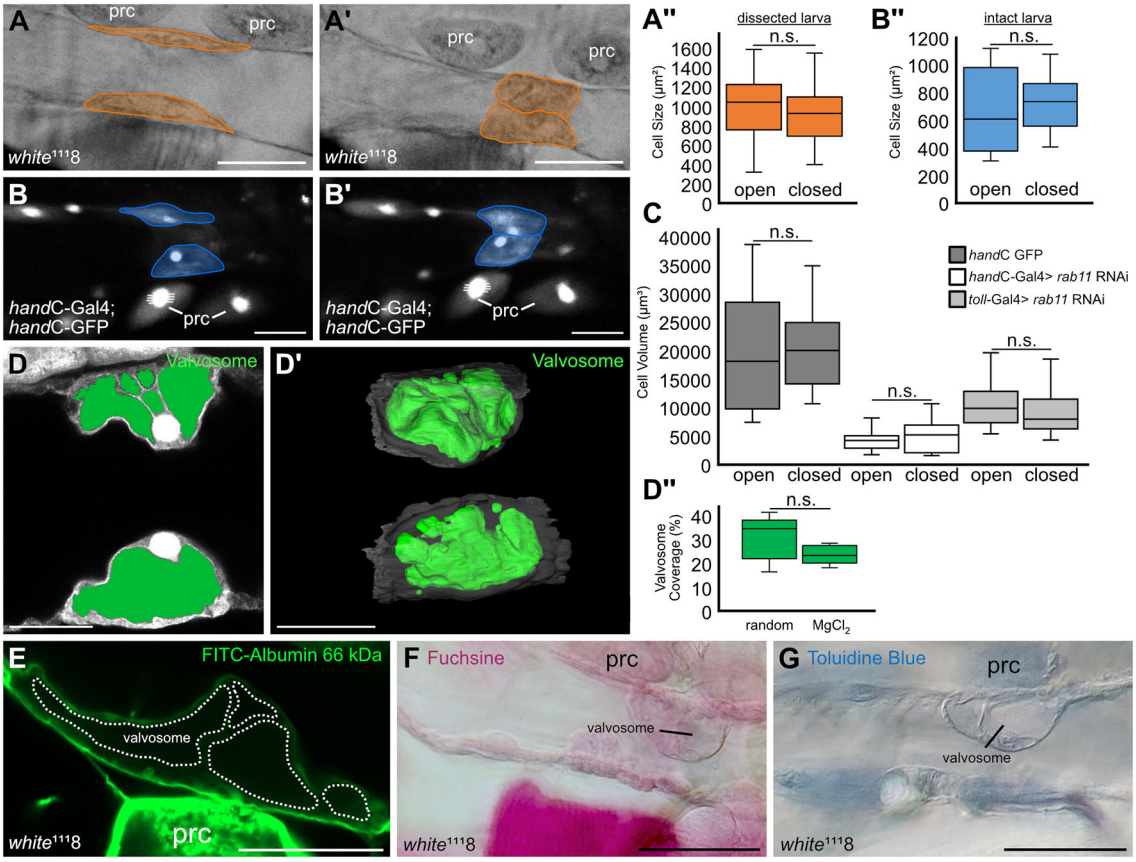

Fig. 6. The volume of valve cells and the valvosomal compartment do not change upon heartbeat. (A-A″) Analysis of the valve cell area of dissected larva from light microscopic videos. The size of the cell does not change between the open and the closed state. (B-B″) Analysis of the valve cell area of intact larva from confocal videos. The size of the cell does not change between the open and the closed state. (C) Calculated valve cell volume from confocal images assuming an ellipsoid valve cell shape and a tubular heart. The volume of the cell does not change during heart beat in control flies and *rab11* knockdown flies but the cell volume of *rab11* knockdown animals is significantly reduced. (D-D″) 3D reconstruction of valve cells and valvosomal compartment in an intermediate state and closed state. There is no difference in the proportion of the valvosomal compartment between the open and closed state. (E-G) Dye uptake of valve cells and the valvosomal compartment. FITC-Albumin, Fuchsine and Toluidine Blue can be found in the cytoplasm of valve cells but not in the valvosome. Scale bars: 50 µm in A-B′,F,G; 25 µm in D-E. **P*<0.05, ***P*<0.01, ****P*<0.001.

measurement accuracy (Fig. 4K). Next, we measured the mean pixel intensity of the PIP reporter genes in comparison with α-Spectrin as a reference for normalisation, and compared the α-Spectrin/PIP ratio in the plasma and valvosome membranes of the same cells (Fig. 4J-M). We found that both PIP2 and PIP3 were significantly enriched in the valvosomal membrane (about 1.3 times), compared with the plasma membrane (Fig. 4L,M), demonstrating a rather high level of these PIPs within the membrane of valvosomes.

To further support the model that valvosomes represent derivatives of the plasma membrane and that the PIP composition is a crucial determinant of this nature, we analysed the effects of modulating PIP concentrations. In this regard, we used RNAi-mediated knockdown to interfere with phospholipid biosynthesis, aiming to alter – to some extent – the PIP signature of the membrane. Indeed, downregulation of the PIP5-kinase Skittles, which potentially inhibits synthesis of PIP2 (Hassan et al., 1998), resulted in formation of additional valvosomes, but had no effect on cell size (Fig. S3).

Together with our data on phosphoinositide distribution, these results support the hypothesis that valvosome and plasma membranes exhibit similar biochemical properties, and that the Spectrin cytoskeleton might be required to mechanically stabilise valvosomes. At this point, we postulate that the valvosomal compartment constitutes a derivative of the plasma membrane, which originates by endocytosis, and is maintained by continuous fusion events with recycling endosomes that occur in a Rab11-dependent manner.

Valvosomes constitute continuations of the plasma membrane

A feasible explanation for the similar lipid signatures of plasma and valvosomal membranes would be that the membranous cavities of the valvosomes represent continuations of the plasma membrane. In other words, valvosomes may originate from incomplete plasma membrane tubulation events. If so, we expected (1) that the membrane of the valvosome would maintain a direct connection with the plasma membrane; (2) that the lumen of the valvosome itself would represent the extracellular space; and (3) that membrane tubulation events would be observed during the differentiation of valve cells.

Indeed, in EM sections of the embryonic progenitors of valve cells, we observed membrane invagination events during development. We found multiple invaginations, starting from the luminal side of the cell. Furthermore, it seems that material from the extracellular matrix were engulfed by the forming valvosomes (Fig. S4). To assess this hypothesis in detail, we systematically

Development (2022) 149, dev200701. doi:10.1242/dev.200701

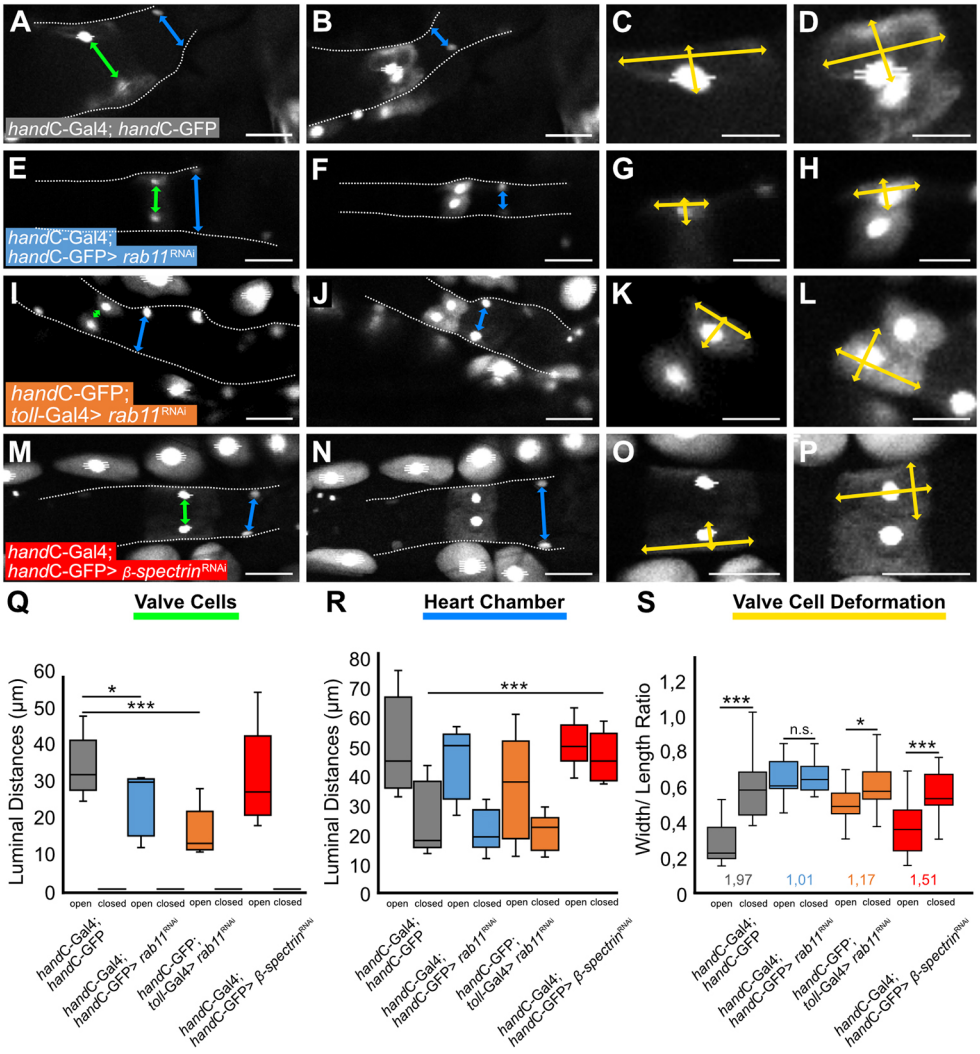

Fig. 7. Absence of valvosomes affects valve cell deformability and the luminal diameter of the heart. (A,B) *hand*C GFP control line. During heartbeat, valve cells switch between an elongated shape (open state, A) and a spherical shape (closed state, B). Green double-headed arrow indicates point of measurement for luminal distance between opposing valve cells and blue double-headed arrows indicates point of measurement for luminal distance within the heart chamber. (C,D) Magnifications of the two states depicted in A and B; yellow double-headed arrows indicate points of measurement for valve cell deformation. (E-H) *hand*C-driven knockdown of *rab11* leads to absence of the valvosomal compartments. Colouring of double-headed arrows is identical to A-D. (I-L) *toll*-driven knockdown of *rab11* leads to absence of the valvosomal compartments. Colouring of double-headed arrows is identical to A-D. (M-P) *hand*C-driven knockdown of *β-Spectrin*. Colouring of double-headed arrows is identical to A-D. (Q,R) Luminal distances of valve cells (Q) and heart chamber (R) upon heartbeat. In the open state, the luminal distance between valve cells is significantly decreased in *rab11* knockdown animals but not in *β-Spectrin* knockdown animals (Q). The luminal distance within the heart chamber in *rab11* knockdown animals is not affected (R), while *β-Spectrin* knockdown significantly affects luminal distance of the heart chamber. (S) Valve cells of *rab11* and *β-Spectrin* knockdown animals exhibit reduced deformation upon heartbeat compared with control cells (*hand*C-GFP). Coloured numbers indicate the deformation change of mean width/length ratios in the open and the closed state, respectively. RNAi lines: *rab11*, v108382; *β-Spectrin*, v40254. Scale bars: 50 µm in A,B,E,F,I,J,M-P; 25 µm in C,D,G,H,K,L. **P*<0.05, ***P*<0.01, ****P*<0.001.

analysed ultrathin cross-sections of valve cells in larval stages by TEM, and found a few plasma membrane invaginations that continued seamlessly into valvosomes (Fig. 5A,C). The initial plasma membrane invaginations resulted in a pore-like structure that was sealed by a massive accumulation of electron-dense material (Fig. 5B). This material displayed the same structural appearance as the extracellular matrix at the surface of heart cells and remains of ECM could also be found on the luminal surface of the inner valvosomal membrane. To verify that the observed material is indeed formed by ECM proteins, we stained the cross-sections with Ruthenium Red, which strongly binds to glycoproteins and causes an electron-dense contrast in EM sections (Dierichs, 1979; Hayat, 1986). At the sites of invagination, we observed a clear electron-dense staining, that became weaker along the surface of the inner valvosome membrane (Fig. 5C,D). This indicates that the plasma membrane invaginations are indeed filled with ECM material, and that the surface of the inner membrane of valvosomes might be loosely covered by the remains of the ECM. To substantiate this finding, we investigated the distribution of the ECM protein Nidogen/Entactin in valve cells. Under standard imaging conditions, we observed only a weak Nidogen signal; however, overexposure of the microscopic samples clearly showed that Nidogen covered the entire valvosome membrane, although weaker if compared with staining of plasma membranes (Fig. 5E-G). Taken

Development (2022) 149, dev200701. doi:10.1242/dev.200701

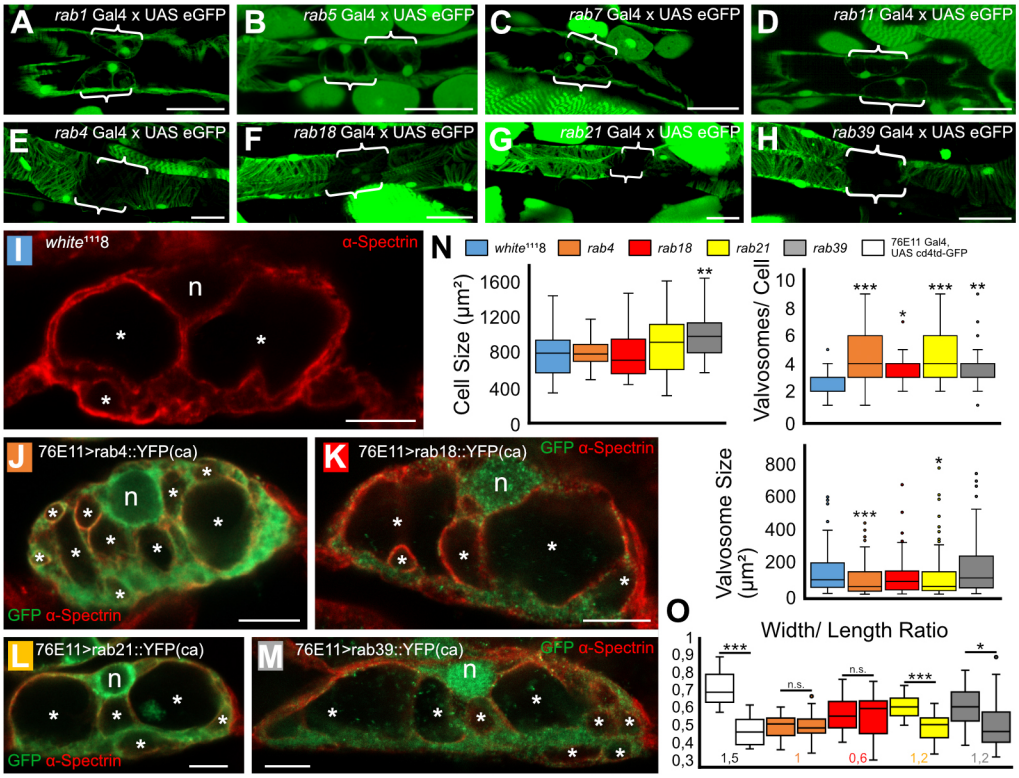

Fig. 8. Four Rab proteins are expressed in all heart cells, except for the valve cells. (A-H) GFP expression driven by *rab*-Gal4 enhancer lines. (A-D) The majority of Rabs are expressed in all heart cells; the expression of Rab1, Rab5, Rab7 and Rab11 is shown as an example (single optical slices). (E-H) The *rab4*, *rab18*, *rab21* and *rab39* enhancers are active in all cardiomyocytes, except for the valve cells (maximum projections). (I-N) Ectopic expression of constitutively active forms of Rabs in valve cells impacts valvosome histology. In all four cases, the number of valvosomes is increased, while their average size is significantly reduced. Confocal images showing the altered histology of valves if constitutively active forms of Rab4, Rab18, Rab21 and Rab39, respectively, are expressed. (O) Ectopic expression of constitutively active forms of Rabs impacts valve cell deformability compared with control animals (white boxplot: 76E11 Gal-4, UAS cd4td-GFP control line). Number of analysed cells: *white*^{1118} (*n*=38), *rab4* (*n*=46), *rab18* (*n*=20), *rab21* (*n*=34) and *rab39* (*n*=48). **P*<0.05, ***P*<0.01, ****P*<0.001. Scale bars: 50 µm in A-H; 10 µm in I-M.

together, the observed tubulation events in valve cell progenitors, as well as the presence of ECM along the valvosome membranes, strongly indicated that the lumen of the valvosome represents extracellular space in the true sense, and is formed by membrane tubulation events.

To further characterise the morphology of the valvosome, we imaged sections of a single pair of valve cells by light microscopy and generated a 3D-rendered model (Fig. 5H-K; Movie 1). We found that, in different cells, the valvosomes occupied about 20% to 65% of the entire cell volume (Fig. S5). To assess this issue more precisely, we generated a three-dimensional dataset of a pair of valve cells using serial block-face EM (SBF-EM). Compared with the light microscopy data, the 3D model obtained by SBF-EM was much more detailed and allowed the analysis of additional smaller organelles in the cytosol of the cells (Fig. 5L-N, Movie 2). This three-dimensional reconstruction also showed that most, if not all, valvosomes are interconnected to each other, and form a single large membrane compartment that is connected to the outer plasma membrane.

Valve cells do not change their volume during heart beat

Previously, we showed that valvosomes ensure the elastic deformability of valve cells, thereby enabling the cells to control directionality and efficient haemolymph flow through the heart (Lammers et al., 2017). Our observation that valvosomes were connected to the extracellular space prompted us to investigate whether these openings have any relevance for the function of valves by allowing the inflow and outflow of haemolymph, and thus a change of the volume of the cell. Therefore, we first imaged larval heartbeat in dissected (Fig. 6A-A″) and intact living animals (Fig. 6B-B″). Valve cells underwent a considerable deformation during each heartbeat, exhibiting a stretched and elongated shape during contraction (open state), and a more rounded shape during relaxation, when the heart lumen is sealed by the valves (closed state, Fig. 6A′,B′). We were able to capture these cell shape changes, using both dissected larvae, as well as a heart-specific GFP reporter (*hand*C-GFP). To obtain a first estimate or whether this deformation also caused a modulation of cell size, we measured the area occupied by the valves in the open as well as closed state in a two-dimensional focal plane. We found that, despite their deformation, the size of the cells did not change over the course of the observation, indicating that the cells maintain their volume over time. Our imaging approaches did not allow the temporal resolution to obtain three-dimensional stacks of beating valve cells. However, in order to estimate the volume of the cells, we used our 2D datasets from beating valve cells of intact animals to calculate an approximate cell volume. Therefore, we assumed an ellipsoid cell shape and a tubular heart tube. Valve cell volume was then calculated as $^{4}/_{3}*\pi*a*b*Z$, with parameters a and b describing the width and length of the cell and Z the depth of the cell. Parameters a and b were directly measured from single frames of live beating valve cells, while parameter Z was calculated using Pythagoras' theorem and the assumption of a tubular heart (Fig. S6). Parameters and, thus, valve cell volume were calculated for each

Development (2022) 149, dev200701. doi:10.1242/dev.200701

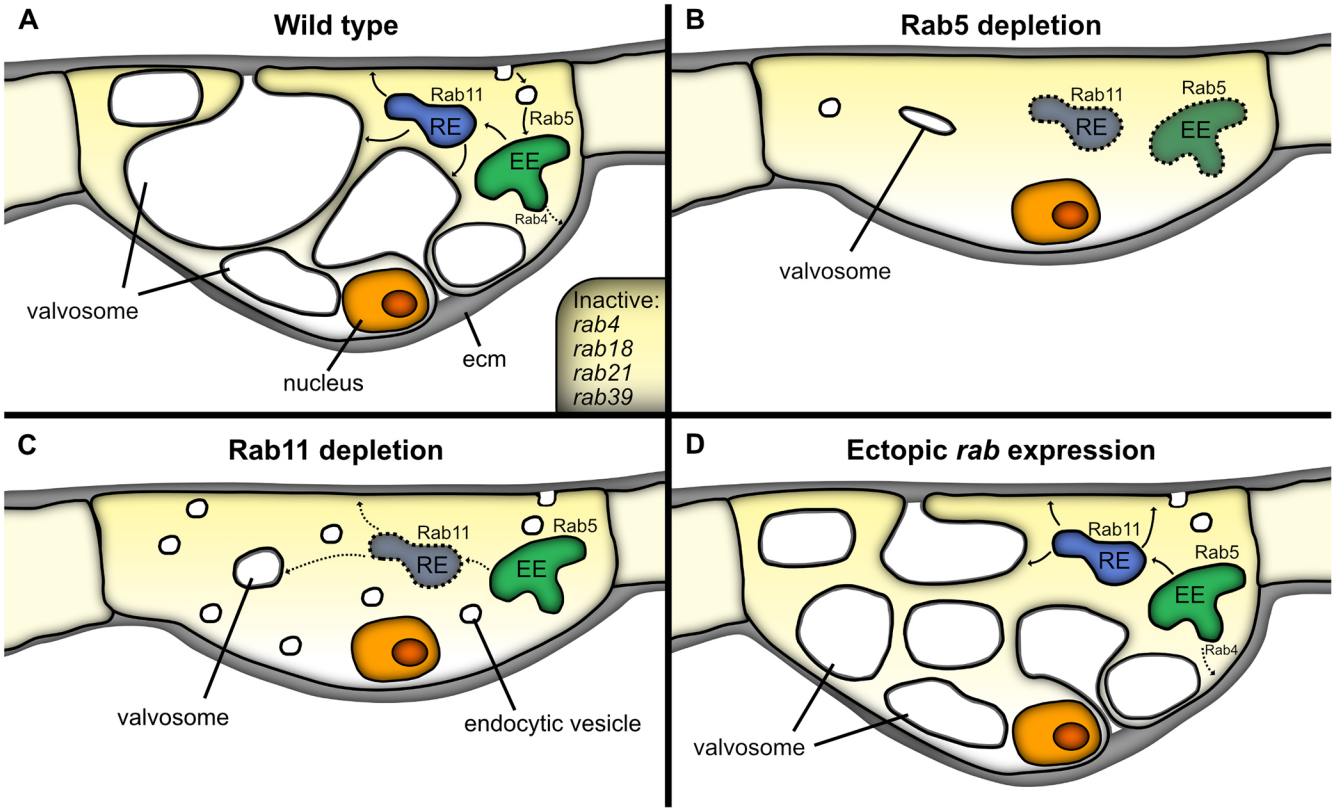

Fig. 9. Schematic representation of our working model. (A) In the wild type, the valvosomal compartment is formed by membrane tubulation (incomplete endocytosis) and maintained by redirecting vesicles from the Rab11-dependent recycling endosomal pathway to the valvosome. Recycling endosomes are targeted to the valvosomal membrane based on its plasma membrane signature. (B,C) Interfering with endocytosis by knockdown of *rab5* or with the recycling pathway by knockdown of *rab11* inhibits valvosome formation. (D) Ectopic expression of constitutively active *rab4*, *rab18*, *rab21* or *rab39* GTPases impairs valvosome histology, probably by consuming membrane material that is normally required for valvosomal growth and maintenance.

valve cell in the open and closed state, respectively. We found that the estimated volume of the valve cells did not change over time, validating our results regarding the cell area (compare Fig. 6C with Fig. 6A″,B″). Next, we tested whether the depletion of *rab11* would result in a change in behaviour of the cells during heartbeat. Although the cells were considerably smaller than their wild-type counterparts, the approximated volume remained constant during heart beat (Fig. 6C). Together, this indicated that valve cells dynamically deform but do not change their absolute volume during heartbeat, excluding the idea of a fluid exchange between the lumen of the valvosome and the external medium. To solidify these observations, we measured the volume of the valvosome itself from confocal stacks of fixed animals. When fixed at random time point during heartbeat, the valvosomes occupied about 15-40% of the volume of a cell (Fig. 6D-D″). To lock cells in a relaxed state, we treated dissected animals with $MgCl_2$ before fixation, which resulted in the relaxation of all striated muscles. Compared with the randomly fixed animals, valvosomes did not significantly change their volume in relation to cell size. In conclusion, this shows that valvosome size, as well as the sizes of the cells, stay constant during heartbeat. Finally, we tested whether there is fluid exchange between the lumen of the valvosomes and the extracellular fluid. We treated dissected heart with different dyes, including a 66 kDa heavy FITC-coupled albumin, as well as the soluble dyes Fuchsine and Toluidine Blue. None of the dyes tested was able to flow into the valvosome lumen, thus clearly showing that the connection between the valvosome and the body cavity is sealed (Fig. 6E-G).

Taken together, our experiments confirmed that the valve cells control heart lumen diameter, thus regulating haemolymph flow within the heart by mechanical deformation and not by a passive or active change in their volume. However, the question remained of how the identified vesicle trafficking pathways and the changed morphology of the valvosomes affect their deformability.

Absence of valvosomes affects valve cell deformability and heart lumen closure characteristics

In order to better describe the deformation of valve cells during heartbeat, we used live imaging of intact animals, carrying the heart-specific *hand*C-GFP reporter line. To assess the closing state of the heart, we measured the distance between valve cells in the open and the closed state of the valve, as well as the adjacent cardiomyocytes (Fig. 7). To extract the deformability of the valve cells, we calculated the width to length ratio of the valve cells in the same conditions (Movies 3 and 4). This allowed us to directly investigate the impact of valvosomes on the elastic deformability of the cells in living animals. First, we measured the distance between opposing valve cells (luminal diameter), as well as between the cells forming the posterior heart chamber, in fully contracted (open state) and fully relaxed (closed state) hearts (Fig. 7A-D,Q-S). We found that absence of the valvosomes in *rab11*-depleted cells resulted in a significantly reduced luminal diameter between the valve cells, relative to wild type (Fig. 7E-H,Q). The luminal diameter between cells forming the heart chamber was not affected (Fig. 7R). However, valve cells lacking valvosomes were still able to close the heart lumen at the fully relaxed state (Fig. 7Q). Next, we analysed

Development (2022) 149, dev200701. doi:10.1242/dev.200701

the deformability of the valve cells in *rab11*-depleted and in control flies (Fig. 7E-H,S). We found, that valve cells that lack valvosomes do not deform as efficiently as their wild-type counterparts, which likely reflects reduced elastic deformability (Fig. 7S). Whereas wild-type valve cells stretch out during the opening of the heart lumen (width-to-length ratio increased approximately 100%), *rab11*-depleted cells fail to deform, and the width-to-length ratio does not change. This was also true when *rab11* was knocked down in a valve cell-specific manner, demonstrating cell-autonomous function of Rab11 in valve cells (Fig. 7I-L,S). Reduced elastic deformability was also observed upon knockdown of β-spectrin (Fig. 7M-P,S). The width-to-length ratio changed by 50%, whereas in wild-type valve cells the decrease was about 100%. In addition, knockdown of β-spectrin significantly impacts luminal distance of the heart chamber (Fig. 7R), but hast no effect on the distance of opposing valve cells (Fig. 7Q).

In summary, these results show that lack of valvosomes, caused by reduced *rab11* expression or by changes in the cell cortex via reduced β-spectrin expression considerably impair the biophysical properties of the valve cells, and thus their physiological functionality.

Valve cells lack expression of *Rab4*, *Rab18*, *Rab21* and *Rab39*

We previously analysed the expression of all known Rab genes in *Drosophila* heart cells (Lammers et al., 2017, this work) and found that valve cells expressed all of them, except for *Rab4*, *Rab18*, *Rab21* and *Rab39* (Fig. 8A-H). Many other Rabs are not expressed at all in cardiac cells, whereas *Rab5*, *Rab7* and *Rab11*, for example, are expressed in all heart cells, including valve cells. Based on these results, we speculated that Rab4, Rab18, Rab21, and Rab39-regulated pathways may be detrimental to valvosome formation, and that, consequently, expression of these particular Rab genes is inhibited in valve cells. To test this hypothesis, we ectopically expressed constitutively active versions of each of these four proteins in valve cells, and analysed the morphology of valvosomes. We found that ectopic expression of any of the four Rab proteins significantly impaired formation of valvosomal compartments in valve cells (Fig. 8I-N). Compared with wild type, valve cell-specific overexpression of constitutively active Rab4, Rab18 and Rab21 resulted in a higher number of smaller valvosomes (Fig. 8N), whereas ectopic expression of Rab39 increased the number of valvosomes without affecting their size (Fig. 8N). We speculate that ectopic activation of the corresponding pathways may consume membrane resources, which normally end up in the valvosome membrane. The reduced supply of these resources would then lead to the observed impairments in valvosome formation or maintenance (Fig. 8). Additionally, we found that expression of constitutively active Rab4, Rab18, Rab21 and Rab39 considerably changed the deformability, and thus mechanical properties, of valve cells (Fig. 8O).

In summary, we conclude that ectopic activation of endosomal pathways that are typically inactive in valve cells hampers proper formation of valvosomes. This result may be based on the possibility that the activated endosomal routes consume membrane resources at the expense of the valvosomes. In consequence, during evolution corresponding pathways may have been inactivated specifically in valve cells, thereby facilitating formation of their unique structure and functionality in the *Drosophila* heart.

DISCUSSION

In this work, we analysed formation and function of a new type of exceptionally large intracellular vesicles, so-called valvosomes. These organelles are essential for the dynamic shape changes that occur for cardiac valve cells during heartbeat. Cells lacking valvosomes lose their deformability and thus their functionality (Fig. 7). Our data indicate that a previously unreported mechanism based on modified activities of well-characterised cellular pathways, governs the formation of these vesicles. We identified two independent cellular processes as being essential for the formation and maintenance of the valvosomes: membrane tubulation and endosome recycling.

We propose that valvosome formation is initiated by Rab5-dependent membrane invagination events. However, unlike endocytosis or phagocytosis, there is no constriction of the internalised region of plasma membrane. Instead, the invagination pore is preserved and sealed with extracellular matrix (Fig. 5A-D). In the second phase, the invaginated membrane grows to its final size by continuous vesicle fusion, and eventually occupies up to two-thirds of the cell volume (Fig. S5). Growth and maintenance seem to be facilitated by recycling endosomes (REs). This is possible because the valvosome membrane is recognised as a target membrane by REs, which continuously supply the growing valvosome with membrane material (Fig. 9).

Of note, the cell has several endosomal recycling routes. One way is through Rab5-dependent early endosomes (EEs) that mature into recycling endosomes (REs) in a Rab11-dependent process. REs sort recycling and retrograde cargoes, which then are transported to the plasma membrane or to the Golgi/ER. This process is referred to as ‘slow recycling’. Some transmembrane proteins can also be transported directly back to the plasma membrane after uptake into an EE, which is called the Rab4-dependent ‘fast recycling’ trafficking pathway (Taguchi, 2013).

However, given our result that Rab4 is not expressed in valve cells (Fig. 8), any involvement of this factor or the ‘fast recycling’ pathway in valvosome formation appears unlikely. On the other hand, Rab11 is expressed in valve cells (Fig. 8) and its downregulation severely impairs valvosome formation (Fig. 2), which strongly indicates that REs of the ‘slow recycling’ pathway provide the membrane resources for the growing valvosome. However, this requires that the membrane of the valvosome is recognised as a preferred target membrane of REs. Our data show that the valvosomal membrane indeed exhibits characteristic properties of a plasma membrane and thus could be recognised by REs: (1) ultrastructural analyses revealed that the valvosome membrane is a direct continuity of the plasma membrane (Fig. 5); (2) the valvosome is decorated with α-Spectrin on its cytoplasmic side, a structural protein that always stabilises the cortex region of plasma membranes, but never decorates intracellular membranes (Fig. 3); (3) we find Nidogen, a protein of the extracellular matrix, at the ‘luminal’ side of valvosomal membranes (Fig. 5E-G); and (4) the lipid signature of the valvosomal membrane mimics the signature of a plasma membrane (Fig. 4). These observations clearly support the idea that the valvosome membrane constitutes a plasma membrane derivative and can be recognised as a target membrane by REs.

It has been shown that the exocysts subunit Sec15 serves as an effector of Rab11 on recycling endosomes, and that the subunits Sec3 and Exo70 tether the complex to the plasma membrane by association with PI(4,5)P_2 (He and Guo, 2009). We found that downregulation of the phosphatidylinositol(4)phosphate 5-kinase *skittles*, which catalyses the conversion of PI(4)P into PI(4,5)P_2, induces an increase of the valvosome number per cell, but has no effect on the cell size, indicating that more but smaller valvosomes are present (Fig. S3). This effect is presumably based on an altered

Development (2022) 149, dev200701. doi:10.1242/dev.200701

lipid signature of the valvosomal membrane, thus emphasising the relevance of proper lipid supply and composition to valvosome formation. Interestingly, we observed a similar phenotype upon downregulation of *sec15*, a core component of the Rab11-binding exocyst complex, where also more but smaller valvosomes were present (Fig. 2). These data suggest that elimination of Skittles results in reduced PI(4,5)P_2 levels in valvosomal membranes, leading to diminished fusion with REs. Upon *sec15* knockdown, the interaction of recycling endosomes and the exocyst complex is likely affected, resulting in a reduced number of REs that are properly tethered to the valvosomes. In both cases, valvosome formation and growth are substantially impaired, probably owing to insufficient access to membrane resources. Similarly, the labyrinth channel system in *Drosophila* nephrocytes also requires Rab11-dependant REs for maintenance, with the PI(4,5)P_2 content in the labyrinth channel membrane being crucial for the recognition by the exocyst complex (Gass et al., 2022; Wen et al., 2020).

Membrane resources

Although we do not yet know whether the valvosome loses membrane material via endocytosis, a dynamic balance between membrane loss by endocytosis and membrane gain by fusion with REs appears likely. As membrane gain is essential for valvosome growth, it is conceivable that non-essential membrane-consuming endomembrane pathways might be inactivated in valve cells. Our data show that this is the case for Rab4-, Rab18-, Rab21- and Rab39-dependent trafficking pathways (Fig. 7E-H). But why are these four Rabs specifically inactivated?

Rab4 is involved in the regulation of AP-1-dependent clathrin-coated vesicle formation at the early endosome (EE) (Pagano et al., 2004) and is thereby responsible for the formation of REs from EEs. Thus, an active Rab4 recycling pathway would compete with the Rab11-dependent pathway, thereby depleting the membrane resources required for valvosome formation and growth. In polarised epithelial cells, Rab18 associates with endocytic structures and localises to membranes near the apical surface (Lutcke et al., 1994). However, there is also evidence for a role in vesicle tethering, secretion and autophagy and for a relationship with the endoplasmic reticulum (Dejgaard and Presley, 2019). Thus, Rab18 appears to be involved in a variety of vesicular pathways consuming membrane material that might be required for valvosomal growth. Rab21 is predominantly dedicated to the early endocytic pathway and expression of protein variants affects endosome morphology and function (Simpson et al., 2004). Cells overexpressing Rab21 display enlarged early endosomes destined for the EE to LE maturation pathway (D'Arrigo et al., 1997; Kauppi et al., 2002). An increased membrane requirement for such EEs could again be at the expense of valvosomes. The same is true for Rab39, which regulates intracellular membrane trafficking pathways, and appears to be involved in cellular endocytosis by regulating endocytic vesicle fusion with the Golgi (Chano and Avnet, 2018; Chen et al., 2003). Inactivation of these membrane-consuming pathways, which are obviously dispensable for the viability of valve cells (Fig. 7E-H), may represent an evolutionary adaptation that allows formation of the valvosomes, and thereby proper development and function of valve cells in the *Drosophila* heart.

Team players: membrane tubulation and recycling endosomes – a win-win situation in many cells?

Is the combination of membrane tubulation and organelle growth by RE fusion a general solution to establish specialised cellular adaptations beyond valvosome formation? Recently, it was discovered that such a system is indeed used for the maintenance of labyrinth channels in nephrocytes. Nephrocytes are endocytically highly active cells, responsible for the uptake and disposal of metabolic waste products and toxins from the haemolymph (Das et al., 2008; Dehnen et al., 2020; Helmstädter and Simons, 2017; Ivy et al., 2015; Weavers et al., 2009). Endocytosis occurs within a lacuna-like channel system formed by membrane invaginations. The stability of the lacuna system is ensured by cell-adhesion molecules at the entrances to the labyrinth channels. Nephrins and other proteins known from podocyte diaphragms form the connections (Martin and Jones, 2018; Zhuang et al., 2009). The labyrinth system, the membranes of which always remain connected to the plasma membrane, provides an enormous increase in surface area available for endocytic uptake of substances. Recent work has shown that cargo receptors of the labyrinth membrane, such as Cubulin and Amnionless, and associated membrane material are recycled to the labyrinth membrane via a Rab11-dependent RE pathway (Wen et al., 2020). Knockdown of components of the Rab11-dependant recycling pathway leads to absence of labyrinth channels and renders nephrocytes non-functional. Moreover, PI(4,5)P_2 is present at the adhesive slit diaphragm of lacuna channels in nephrocytes and a reduction of the lipid by downregulation of its kinase *skittles* prevents slit diaphragm formation (Gass et al., 2022). These results are highly similar to the impaired formation of valvosomes that we observed as a result of *rab11* or *skittles* knockdown (Fig. 2, Fig. S3).

Another example of membrane tubulation is found during the formation of the first epithelial cell layer during early embryogenesis. This process is referred to as cellularisation. It has been shown that, after initial actin-driven membrane invaginations, Rab11-positive recycling endosomes are again required to mobilise vesicular membrane pools and to ensure lateral membrane growth (Pelissier et al., 2003).

The formation of valvosomes, the formation of labyrinth channels and embryonic cellularisation are three examples of basic cellular mechanisms that, if properly modified, establish highly specialised subcellular compartments as an adaptation to specialised cellular functions. In this work, we show for the first time how a specific type of large intracellular vesicle, the valvosome, is generated and maintained in valve cells of the *Drosophila* heart. We postulate that a combination of Rab5-dependent membrane invagination events that lack a vesicle constriction step, and the continuous supply of membrane material to the growing organelle by Rab11-positive endosomes represent the fundamental molecular mechanisms for the generation an maintenance of valvosomes. In addition, absence of distinct endosomal trafficking pathways appears to be essential for valvosome formation, probably as a means to prevent expenditure of required membrane material.

Although a number of questions remain to be addressed, the present study provides valuable data on the formation, maintenance and function of a novel type of cellular organelle: the valvosome. Future studies will reveal to what extent the pathways that govern valvosome maturation are also relevant to the formation of other specialised membrane structures.

MATERIALS AND METHODS

Fly stocks and genetics

The *hand*-Gal4, *toll*-Gal4 and *hand*C-GFP lines used in this study were made by our laboratory (Sellin et al., 2006). The *toll*-GFP line was provided by Robert Schulz (University of Notre Dame, IN, USA) (Wang et al., 2005). The PIP2 marker line Pleckstrin domain::GFP from PhospholipaseC::GFP was obtained from Hugo J. Bellen (Baylor College, TX, USA) and the PIP marker Pleckstrin_domain::GFP from Grp1 was from Bruce Edgar

Development (2022) 149, dev200701. doi:10.1242/dev.200701

(University of Utah, USA). The *rab1*-Gal4, *rab4*-Gal4, *rab5*-Gal4, *rab7*-Gal4, *rab11-Gal4, rab18*-Gal4, *rab21*-Gal4 and *rab39*-Gal4 lines were obtained from Robin Hiesinger (Freie Universität Berlin, Germany). The following lines were obtained from the Bloomington *Drosophila* Stock Center (BDSC) at Indiana University: rab5::YFP (RRID:BDSC_62543), rab7::YFP (RRID:BDSC_62545), rab11:YFP (RRID:BDSC_62549), UAS-Lamp1::GFP (RRID:BDSC_42714), UAS-Atg8a::GFP-mCherry (RRID:BDSC_37749), Golgi EYFP (RRID:BDSC_7193), 76E11-Gal4 (RRID:BDSC_39933), UAS-Rab4pQ67L (RRID:BDSC_9770), UAS-Rab18pA64L (RRID:BDSC_9797), UAS-Rab21pQ73L (RRID:BDSC_23864), UAS-Rab39pQ69L (RRID:BDSC_9823), UAS-eGFP (RRID:BDSC_5428), UAS-mCD8::GFP (RRID:BDSC_5137), UAS-cd4td::GFP (RRID:BDSC_35836), UAS-FYVE::GFP (RRID:BDSC_42712) (Simonsen et al., 1998), alpha-Tub84B>PH Grp1::GFP (RRID:BDSC_8163) and UAS-PLCdelta-PH-eGFP (RRID:BDSC_39693).

The following RNAi lines were obtained from the VIENNA *Drosophila* Resource Center (v) or Bloomington *Drosophila* Stock Center (BL): *rab5* v103945; v34096, *rab7* v40337; BL27051, *rab11* v108382; v22198, *sec15* v105126; v35161 and *spectrin* v42054; v42053.

As a control strain, *white*^{1118} was used. Fly husbandry was carried out as described previously (Wang et al., 2012).

Antibodies and reagents

Antibodies were used to detect Rab7 (1:10; Developmental Studies Hybridoma Bank, USA), Spectrin (1:20; Developmental Studies Hybridoma Bank, USA), Calnexin (1:100; Developmental Studies Hybridoma Bank, USA) and Nidogen (1:1000; a gift from Stefan Baumgartner, Gothenburg, Sweden). Monoclonal rabbit anti-GFP (1:2000) was from Abcam (Ab6556), monoclonal mouse anti-GFP (3E6, 1:500) was from Invitrogen (A-11120; Thermo Fisher Scientific). LysoTracker Red DND-99 and Phalloidin TRITC were from Thermo Fisher Scientific. Secondary antibodies used were anti-mouse Cy2, anti-mouse Cy3 and anti-rabbit Cy2 (1:200; Dianova, Germany).

Immunostaining of valve cells of third instar larvae

Third instar wandering larvae were dissected following previously published protocols (Lehmacher et al., 2012, 2009). Briefly, animals were pinned down on their dorsal side on a Sylgard plate (Sylgard 184, Dow Corning), covered with PBS and opened ventrally along the posterior-anterior axis. Viscera were carefully removed, and specimens were fixed for 1 h at room temperature in 4% methanol-free paraformaldehyde. After three washing steps in BBT for 10 min each, samples were permeabilised with 1% Triton in PBS for 1 h, followed by three additional washing steps in BBT for 10 min each. Afterwards, nonspecific epitopes were blocked by incubation in saturation buffer (1× PBS, 0.1% Tween-20 and 3% BSA) for 1 h at room temperature.

Primary antibodies were diluted in PBS buffer and incubated overnight at 4°C under constant shaking before the solution was removed and replaced by BBT buffer containing 1% Tween for thorough washing to remove unbound antibodies. Secondary antibodies, with coupled fluorophores, were diluted in PBS and incubated at room temperature in the dark for 2 h. All unbound antibodies were finally removed by three washing steps in PBS. Finally, samples were embedded in Fluoromount-GTM (Thermo Fisher Scientific) with DAPI or RotiMount FluorCare with DAPI (Roth) and imaged with a Zeiss LSM 800 laser scanning microscope. Images were analysed using Fiji ImageJ software.

Live imaging of valve cells of third instar larvae

Third instar wandering larvae were placed on a Sylgard plate with their dorsal side facing up and carefully locked in place by two needles on the very anterior and very posterior end. Animals were cleaned of remaining food particles using a fine wet brush and paper tissue. After a resting time of 1 min, specimens were directly analysed with a Zeiss LSM 800 laser scanning microscope. For each animal, videos of 10 s were captured with an acquisition speed of ∼81 ms per frame. Recordings were further processed using Fiji ImageJ software. For valve cell dynamics, the maximal width and length of the valve cells was measured in the closed and open state. Luminal distance was measured as the smallest distance between the valve cells and the cells posterior to the valve cells. Valve cell size was measured as the area (µm²) at the nucleus plane. Three animals per genotype and three heart beats for each animal were analysed. Volume calculation of valve cells from live imaging videos is possible assuming an ellipsoid shape of valve cells and a circular heart tube. Ellipsoid volume was calculated as $\frac{4}{3}*\pi*a*b*Z$. Factors *a* and *b*, determining the width and length of the cell, were measured in the closed and open state, respectively. Factor *Z*, describing the height of the cell, was calculated by measuring the radius of the heart tube at the position of the valve cells in the closed and open state, and applying the Pythagoras' theorem (see Fig. S6). All data were analysed using Fiji ImageJ software and differences were analysed using an unpaired two-tailed Student's *t*-test.

Live imaging of valve cells of dissected third instar larvae

For bright-field live recordings of valve cells, third instar wandering larvae were prepared as described previously (Lammers et al., 2017). For analyses of valve cell size, single frames from recordings with an acquisition speed of 200 frames per second were used. Valve cell area (µm²) in the open and closed state was calculated for 19 larvae using Fiji ImageJ software, and differences were analysed using an unpaired two-tailed Student's *t*-test.

TEM

Specimens were prepared as previously described (Beyenbach et al., 2020; Lehmacher et al., 2012; Psathaki et al., 2018; Rotstein et al., 2018). Briefly, specimens were dissected in PBS, fixed for 4 h at room temperature in fixative composed of 2% glutaraldehyde (Sigma-Aldrich) and 4% paraformaldehyde (Merck) in PBS and post-fixed for 1 h at 4°C in 1% osmium tetroxide in PBS (Sciences Services). Afterwards, samples were dehydrated stepwise in a graded ethanol series followed by 100% acetone. Specimens were embedded in Epon 812 (Merck) and polymerised for 48 h at 60°C. Ultrathin sections (70 nm) were cut on an ultramicrotome (UC6 and UC7, Leica) and mounted on formvar-coated copper slot grids. Sections were stained for 30 min in 2% uranyl acetate (Sciences Services) and for 20 min in 3% lead citrate (Roth). All samples were analysed at 80 kV with a Zeiss 902 or Zeiss LEO912, or at 200 kV with a Jeol JEM2100-Plus transmission electron microscope.

SBF-SEM

Samples were fixed 1 h in 2.5% glutaraldehyde in 0.1 M cacodylate buffer (pH 7.4). Subsequently, the specimens were processed via rOTO-post-fixation and embedded in Epon, ensuring pronounced contrast and electron dose resistance for consecutive imaging (Deerinck et al., 2010). The polymerised sample was further trimmed and sectioned to locate the ROI. Once an adequate region was confirmed, the Epon block was trimmed to a block of 300 µm³ and glued onto an aluminium rivet using silver conductive epoxy adhesive. The sample was further sputter-coated with 30 nm gold using a Leica ACE-600 sputter coater and mounted into the chamber of a JEOL 7200-F scanning electron microscope equipped with the 3View in-chamber ultramicrotome system stage (Gatan). Image acquisition was performed at an accelerating voltage of 3.0 kV, using a condenser aperture of 30 nm in a high-pressure vacuum of 10 Pa. Resolution of the respective image series of 22.7 nm was in *x* and *y* directions (with an image size of 4000×4000 pixels); the slice thickness (*z*-direction) was set to 30 nm. The dwell time of each pixel was set to 32 µs. Overall, 779 individual slices were imaged, resulting in an effective volume of 93×93×23 µm.

The dataset was collected with Digital Micrograph Suite (Gatan). Alignment, further processing and segmentation of the stacks were handled using Microscopy Image Browser, MIB, Version 2.6 (Belevich et al., 2016). Cell structures were semi-automatically annotated using the graphcut segmentation tool, refinement of structures was supervised manually. Subsequent three-dimensional image visualisation and analysis were performed using IMARIS software (BitPlane).

Three-dimensional reconstruction of valve cells

For three-dimensional reconstruction of valve cells, samples were processed as described for TEM analysis. Sections (700 nm) were cut with a Leica UC7 ultramicrotome and stained with Toluidine Blue solution. Light microscopic images were taken with a Zeiss Axioskop2 equipped with a Zeiss Axiocam MRc 5 digital camera using the Axiovision software. For

Development (2022) 149, dev200701. doi:10.1242/dev.200701

reconstruction, 84 sections were manually analysed and subsequently rendered into a 3D surface model using Amira 5.0.1 software (Visage Imaging) and 'unconstrained smoothing' option. To calculate the volume of valve cells and valvosomes, confocal stacks were acquired. *Hand*C-GFP expressing animals were prepared as described previously (see section in 'Immunostainings of valve cells of third instar larvae') and stained for GFP and Spectrin. Specimens were randomly fixed (valve cells in transition between the open and closed state) or relaxed for 5 min in $MgCl_2$ (valves in the fully relaxed state) prior to fixation. Volumes of valve cells and valvosomes were calculated using Microscopy Image Browser, MIB, Version 2.6 (Belevich et al., 2016). In total, six cells per condition were analysed.

Valve cell measurements

For statistical analysis of valve cells, confocal sections through the nuclear plane were taken and analysed using Fiji ImageJ software and the 'Polygon selection' tool. The phosphatidylinositol/ Spectrin ratio was measured on sections where the plasma membrane and the valvosome membrane were clearly separated from each other. The 'Rectangle'-tool was used to measure mean grey values. Three different animals were analysed and five measurement points for the plasma membrane and five points for the valvosome membrane were measured in each animal. All data were analysed using an unpaired two-tailed Student's *t*-test.

Dye uptake of valve cells

FITC albumin uptake of third instar larvae was performed as previously described (Dehnen et al., 2020). In brief, larvae were dissected in artificial haemolymph and incubated in 0.2 mg/ml FITC-albumin (A9771; albumin-fluorescein isothiocyanate conjugate; MW 66 kDa; Sigma-Aldrich) for 5 min in the dark, fixed in 3.7% PFA, washed thoroughly and analysed using a Zeiss LSM 800 laser scanning microscope.

For Fuchsine or Toluidine Blue uptake, larvae were dissected in artificial haemolymph and incubated in Toluidine Blue in artificial haemolymph (5 g/100 ml) for 5 s or Fuchsine in artificial haemolymph (0.1 g/100 ml) for 10 s. Staining solution was replaced by 4% FA fixation solution for 15 min and animals were directly observed.

Ruthenium Red staining

For Ruthenium Red staining, larvae were prepared according to previously published protocols (Hayat, 1986). In brief, dissected larvae were fixed and stained with a glutaraldehyde, Ruthenium Red and cacodylate buffer solution for 1 h at room temperature and rinsed in the buffer. Samples were post-fixed in an osmium, Ruthenium Red and cacodylate buffer solution for 3 h at room temperature before dehydration using a graded ethanol series and embedding in Epon.

Data presentation

Data are shown as box plots with lower and upper whiskers representing minimum and maximum distribution, respectively. Boxes represent 50% of data (quartile groups 2 and 3). Lines within boxes represent the median. Lower and upper outliers are shown as single data points and are defined as exceeding a distance of 1.5 times the IQR below the 1st quartile or above the 3rd quartile, respectively.

Acknowledgements

We thank Werner Mangerich for excellent technical assistance. Furthermore, we thank our Master and Bachelor students Franz Kahlich, Judith Peters, Christina Rauf and Sara Timm for supporting us with staining and imaging. We also thank Kerstin Etzold and Ekatherini Psathaki (Z-Project SFB944) for excellent technical assistance and for EM support.

Competing interests

The authors declare no competing or financial interests.

Author contributions

Conceptualization: C.M., A.P.; Methodology: C.M., M.D., H.M., A.P.; Formal analysis: C.M.; Investigation: C.M., L. Breitsprecher; Writing - original draft: C.M., A.P.; Writing - review & editing: C.M., M.D., H.M., A.P.; Visualization: C.M.; Supervision: L. Bataille, A.J.M.V., A.P.; Project administration: A.P.; Funding acquisition: A.P.

Funding

This work was supported by grants from the Deutsche Forschungsgemeinschaft to A.P. (PA 517/13-1 and SFB944), and to L. Bataille (DAAD and Procope).

References

Belevich, I., Joensuu, M., Kumar, D., Vihinen, H. and Jokitalo, E. (2016). Microscopy image browser: a platform for segmentation and analysis of multidimensional datasets. *PLoS Biol.* **14**, e1002340. doi:10.1371/journal.pbio.1002340

Beyenbach, K. W., Schöne, F., Breitsprecher, L. F., Tiburcy, F., Furuse, M., Izumi, Y., Meyer, H., Jonusaite, S., Rodan, A. R. and Paululat, A. (2020). The septate junction protein Tetraspanin 2A is critical to the structure and function of Malpighian tubules in *Drosophila melanogaster*. *Am. J. Physiol. Cell Physiol.* **318**, C1107-C1122. doi:10.1152/ajpcell.00061.2020

Chan, C.-C., Scoggin, S., Wang, D., Cherry, S., Dembo, T., Greenberg, B., Jin, E. J., Kuey, C., Lopez, A., Mehta, S. Q. et al. (2011). Systematic discovery of Rab GTPases with synaptic functions in *Drosophila*. *Curr. Biol.* **21**, 1704-1715. doi:10.1016/j.cub.2011.08.058

Chano, T. and Avnet, S. (2018). RAB39A: a Rab small GTPase with a prominent role in cancer stemness. *J. Biochem.* **164**, 9-14. doi:10.1093/jb/mvy041

Chen, T., Han, Y., Yang, M., Zhang, W., Li, N., Wan, T., Guo, J. and Cao, X. (2003). Rab39, a novel Golgi-associated Rab GTPase from human dendritic cells involved in cellular endocytosis. *Biochem. Biophys. Res. Commun.* **303**, 1114-1120. doi:10.1016/S0006-291X(03)00482-0

D'Arrigo, A., Bucci, C., Toh, B. H. and Stenmark, H. (1997). Microtubules are involved in bafilomycin A1-induced tubulation and Rab5-dependent vacuolation of early endosomes. *Europ. J. Cell Biol.* **72**, 95-103.

Das, D., Aradhya, R., Ashoka, D. and Inamdar, M. (2008). Post-embryonic pericardial cells of *Drosophila* are required for overcoming toxic stress but not for cardiac function or adult development. *Cell Tissue Res.* **331**, 565-570. doi:10.1007/s00441-007-0518-z

Deerinck, T. J., Bushong, E. A., Lev-Ram, V., Shu, X., Tsien, R. Y. and Ellisman, M. H. (2010). Enhancing serial block-face scanning electron microscopy to enable high resolution 3-D nanohistology of cells and tissues. *Microsc. Microanal.* **16**, 1138-1139. doi:10.1017/S1431927610055170

Dehnen, L., Janz, M., Kumar Verma, J., Psathaki, O. E., Langemeyer, L., Fröhlich, F., Heinisch, J. J., Meyer, H., Ungermann, C. and Paululat, A. (2020). A trimeric metazoan Rab7 GEF complex is crucial for endocytosis and scavenger function. *J. Cell Sci.* **133**, jcs247080. doi:10.1242/jcs.247080

Dejgaard, S. Y. and Presley, J. F. (2019). Rab18: new insights into the function of an essential protein. *Cell. Mol. Life Sci.* **76**, 1935-1945. doi:10.1007/s00018-019-03050-3

Dierichs, R. (1979). Ruthenium red as a stain for electron microscopy. Some new aspects of its application and mode of action. *Histochemistry* **64**, 171-187. doi:10.1007/BF00490097

Gass, M. M., Borkowsky, S., Lotz, M.-L., Siwek, R., Schröter, R. H., Nedvetsky, P., Luschnig, S., Rohlmann, A., Missler, M. and Krahn, M. P. (2022). PI(4,5)P2 controls slit diaphragm formation and endocytosis in *Drosophila* nephrocytes. *Cell. Mol. Life Sci.* **79**, 248. doi:10.1007/s00018-022-04273-7

Gatica, D., Lahiri, V. and Klionsky, D. J. (2018). Cargo recognition and degradation by selective autophagy. *Nat. Cell Biol.* **20**, 233-242. doi:10.1038/s41556-018-0037-z

Grosshans, B. L., Ortiz, D. and Novick, P. (2006). Rabs and their effectors: Achieving specificity in membrane traffic. *Proc. Natl. Acad. Sci. USA* **103**, 11821-11827. doi:10.1073/pnas.0601617103

Hassan, B. A., Prokopenko, S. N., Breuer, S., Zhang, B., Paululat, A. and Bellen, H. J. (1998). *skittles*, a *Drosophila* phosphatidylinositol 4-phosphate 5-kinase, is required for cell viability, germline development and bristle morphology, but not for neurotransmitter release. *Genetics* **150**, 1527-1537. doi:10.1093/genetics/150.4.1527

Hayat, M. A. (1986). *Basic Techniques for Transmission Electron Microscopy*. Academic Press.

He, B. and Guo, W. (2009). The exocyst complex in polarized exocytosis. *Curr. Opin. Cell Biol.* **21**, 537-542. doi:10.1016/j.ceb.2009.04.007

Helmstädter, M. and Simons, M. (2017). Using *Drosophila* nephrocytes in genetic kidney disease. *Cell Tissue Res.* **369**, 119-126. doi:10.1007/s00441-017-2606-z

Ivy, J. R., Drechsler, M., Catterson, J. H., Bodmer, R., Ocorr, K., Paululat, A. and Hartley, P. S. (2015). Klf15 is critical for the development and differentiation of *Drosophila* nephrocytes. *PLoS ONE* **10**, e0134620. doi:10.1371/journal.pone.0134620

Kauppi, M., Simonsen, A., Bremnes, B., Vieira, A., Callaghan, J., Stenmark, H. and Olkkonen, V. M. (2002). The small GTPase Rab22 interacts with EEA1 and controls endosomal membrane trafficking. *J. Cell Sci.* **115**, 899-911. doi:10.1242/jcs.115.5.899

Khawar, M. B., Gao, H. and Li, W. (2019). Mechanisms of Acrosome biogenesis in mammals. *Front. Cell. Dev. Biol.* **7**, 195. doi:10.3389/fcell.2019.00195

LaJeunesse, D. R., Buckner, S. M., Lake, J., Na, C., Pirt, A. and Fromson, K. (2004). Three new *Drosophila* markers of intracellular membranes. *BioTechniques* **36**, 784-788, 790. doi:10.2144/04365ST01

Lammers, K., Abeln, B., Hüsken, M., Lehmacher, C., Psathaki, O. E., Alcorta, E., Meyer, H. and Paululat, A. (2017). Formation and function of intracardiac valve cells in the *Drosophila* heart. *J. Exp. Biol.* **220**, 1852-1863. doi:10.1242/jeb.156265

Langemeyer, L., Fröhlich, F. and Ungermann, C. (2018). Rab GTPase function in endosome and lysosome biogenesis. *Trends Cell Biol.* **28**, 957-970. doi:10.1016/j.tcb.2018.06.007

Lehmacher, C., Tögel, M., Pass, G. and Paululat, A. (2009). The *Drosophila* wing hearts consist of syncytial muscle cells that resemble adult somatic muscles. *Arthropod Struct. Dev.* **38**, 111-123. doi:10.1016/j.asd.2008.09.002

Lehmacher, C., Abeln, B. and Paululat, A. (2012). The ultrastructure of *Drosophila* heart cells. *Arthropod Struct. Dev.* **41**, 459-474. doi:10.1016/j.asd.2012.02.002

Lin, J. Y. and Fisher, D. E. (2007). Melanocyte biology and skin pigmentation. *Nature* **445**, 843-850. doi:10.1038/nature05660

Lutcke, A., Parton, R. G., Murphy, C., Olkkonen, V. M., Dupree, P., Valencia, A., Simons, K. and Zerial, M. (1994). Cloning and subcellular localization of novel rab proteins reveals polarized and cell type-specific expression. *J. Cell Sci.* **107**, 3437-3448. doi:10.1242/jcs.107.12.3437

Martin, C. E. and Jones, N. (2018). Nephrin Signaling in the Podocyte: An updated view of signal regulation at the slit diaphragm and beyond. *Front. Endocrinol.* **9**, 302. doi:10.3389/fendo.2018.00302

Maxfield, F. R. and McGraw, T. E. (2004). Endocytic recycling. *Nat. Rev. Mol. Cell. Biol.* **5**, 121-132. doi:10.1038/nrm1315

Pagano, A., Crottet, P., Prescianotto-Baschong, C. and Spiess, M. (2004). *In vitro* formation of recycling vesicles from endosomes requires adaptor protein-1/clathrin and is regulated by rab4 and the connector rabaptin-5. *Molec. Biol. Cell* **15**, 4990-5000. doi:10.1091/mbc.e04-04-0355

Pelissier, A., Chauvin, J.-P. and Lecuit, T. (2003). Trafficking through Rab11 endosomes is required for cellularization during *Drosophila* embryogenesis. *Curr. Biol.* **13**, 1848-1857. doi:10.1016/j.cub.2003.10.023

Psathaki, O.-E., Dehnen, L., Hartley, P. S. and Paululat, A. (2018). *Drosophila* pericardial nephrocyte ultrastructure changes during ageing. *Mech. Ageing Dev.* **173**, 9-20. doi:10.1016/j.mad.2018.04.006

Rotstein, B., Post, Y., Reinhardt, M., Lammers, K., Buhr, A., Heinisch, J. J., Meyer, H. and Paululat, A. (2018). Distinct domains in the matricellular protein Lonely heart are crucial for cardiac extracellular matrix formation and heart function in *Drosophila*. *J. Biol. Chem.* **293**, 7864-7879. doi:10.1074/jbc.M117.817940

Sellin, J., Albrecht, S., Kölsch, V. and Paululat, A. (2006). Dynamics of heart differentiation, visualized utilizing heart enhancer elements of the *Drosophila melanogaster* bHLH transcription factor Hand. *Gene Expr. Patterns* **6**, 360-375. doi:10.1016/j.modgep.2005.09.012

Setterberg, I. E., Le, C., Frisk, M., Perdreau-Dahl, H., Li, J. and Louch, W. E. (2021). The physiology and pathophysiology of T-tubules in the heart. *Front. Physiol.* **12**, 718404. doi:10.3389/fphys.2021.718404

Sheff, D. R., Daro, E. A., Hull, M. and Mellman, I. (1999). The receptor recycling pathway contains two distinct populations of early endosomes with different sorting functions. *J. Cell Biol.* **145**, 123-139. doi:10.1083/jcb.145.1.123

Simonsen, A., Lippe, R., Christoforidis, S., Gaullier, J.-M., Brech, A., Callaghan, J., Toh, B.-H., Murphy, C., Zerial, M. and Stenmark, H. (1998). EEA1 links PI(3)K function to Rab5 regulation of endosome fusion. *Nature* **394**, 494-498. doi:10.1038/28879

Simpson, J. C., Griffiths, G., Wessling-Resnick, M., Fransen, J. A. M., Bennett, H. and Jones, A. T. (2004). A role for the small GTPase Rab21 in the early endocytic pathway. *J. Cell Sci.* **117**, 6297-6311. doi:10.1242/jcs.01560

Skalak, R. and Chien, S. (1982). Rheology of blood cells as soft tissues. *Biorheology* **19**, 453-461. doi:10.3233/BIR-1982-19306

Spang, A. (2016). Membrane tethering complexes in the endosomal system. *Front. Cell. Dev. Biol.* **4**, 35. doi:10.3389/fcell.2016.00035

Stokke, B. T., Mikkelsen, A. and Elgsaeter, A. (1986). Spectrin, human erythrocyte shapes, and mechanochemical properties. *Biophys. J.* **49**, 319-327. doi:10.1016/S0006-3495(86)83644-X

Taguchi, T. (2013). Emerging roles of recycling endosomes. *J. Biochem.* **153**, 505-510. doi:10.1093/jb/mvt034

Ullrich, O., Reinsch, S., Urbé, S., Zerial, M. and Parton, R. G. (1996). Rab11 regulates recycling through the pericentriolar recycling endosome. *J. Cell Biol.* **135**, 913-924. doi:10.1083/jcb.135.4.913

Volpatti, J. R., Al-Maawali, A., Smith, L., Al-Hashim, A., Brill, J. A. and Dowling, J. J. (2019). The expanding spectrum of neurological disorders of phosphoinositide metabolism. *Dis. Model. Mech.* **12**, dmm038174. doi:10.1242/dmm.038174

Wang, J., Tao, Y., Reim, I., Gajewski, K., Frasch, M. and Schulz, R. A. (2005). Expression, regulation, and requirement of the Toll transmembrane protein during dorsal vessel formation in *Drosophila melanogaster*. *Mol. Cell Biol.* **25**, 4200-4210. doi:10.1128/MCB.25.10.4200-4210.2005

Wang, S., Meyer, H., Ochoa-Espinosa, A., Buchwald, U., Önel, S., Altenhein, B., Heinisch, J. J., Affolter, M. and Paululat, A. (2012). GBF1 (Gartenzwerg)-dependent secretion is required for *Drosophila* tubulogenesis. *J. Cell Sci.* **125**, 461-472. doi:10.1242/jcs.092551

Weavers, H., Prieto-Sánchez, S., Grawe, F., Garcia-López, A., Artero, R., Wilsch-Bräuninger, M., Ruiz-Gómez, M., Skaer, H. and Denholm, B. (2009). The insect nephrocyte is a podocyte-like cell with a filtration slit diaphragm. *Nature* **457**, 322-326. doi:10.1038/nature07526

Wen, P., Zhang, F., Fu, Y., Zhu, J.-Y. and Han, Z. (2020). Exocyst genes are essential for recycling membrane proteins and maintaining slit diaphragm in *Drosophila* nephrocytes. *J. Am. Soc. Nephrol.* **31**, 1024-1034. doi:10.1681/ASN.2019060591

Wu, S., Mehta, S. Q., Pichaud, F., Bellen, H. J. and Quiocho, F. A. (2005). Sec15 interacts with Rab11 via a novel domain and affects Rab11 localization *in vivo*. *Nat. Struct. Mol. Biol.* **12**, 879-885. doi:10.1038/nsmb987

Zerial, M. and McBride, H. (2001). Rab proteins as membrane organizers. *Nat. Rev. Mol. Cell. Biol.* **2**, 107-117. doi:10.1038/35052055

Zhang, X.-M., Ellis, S., Sriratana, A., Mitchell, C. A. and Rowe, T. (2004). Sec15 is an effector for the Rab11 GTPase in mammalian cells. *J. Biol. Chem.* **279**, 43027-43034. doi:10.1074/jbc.M402264200

Zhuang, S., Shao, H., Guo, F., Trimble, R., Pearce, E. and Abmayr, S. M. (2009). Sns and Kirre, the *Drosophila* orthologs of Nephrin and Neph1, direct adhesion, fusion and formation of a slit diaphragm-like structure in insect nephrocytes. *Development* **136**, 2335-2344. doi:10.1242/dev.031609

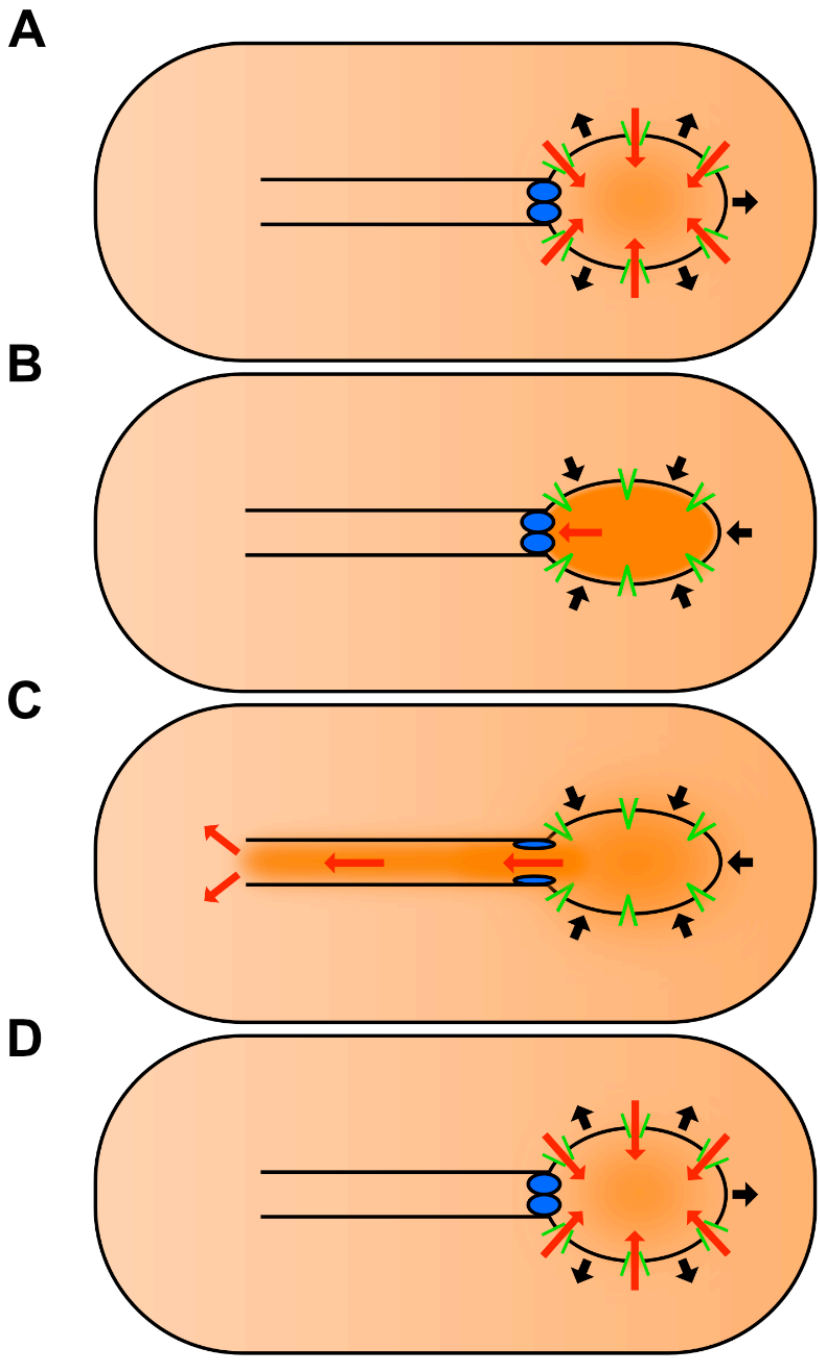

Fig. S1. Model of a contraction cycle of the larval heart. (A) Heart beat initiates by widening of the heart chamber, sucking in haemolymph (red arrows) via open ostia (green lines). Muscles of valve cells are relaxed, the valvosomal compartment defines the roundish shape of the cell (blue ellipses), allowing mechanical contact to the opposing valve cell and thereby an effective closing of the heart lumen. (B) Contraction wave starts posteriorly with contraction of the heart chamber leading to a closing of the ostia cells and an increasing pressure of the haemolymph inside the heart chamber against the still closed valve cells. (C) Contraction wave reaches valves cells leading to a deformation of these cells from roundish to an elongated shape due to the presence of the valvosomal compartment and a dense myofiber network in these cells. Haemolymph is pumped towards the anterior end and valves close the heart lumen directly after the contraction wave proceeds. (D) A new contraction cycle starts with widening of the heart chamber and haemolymph entrance.

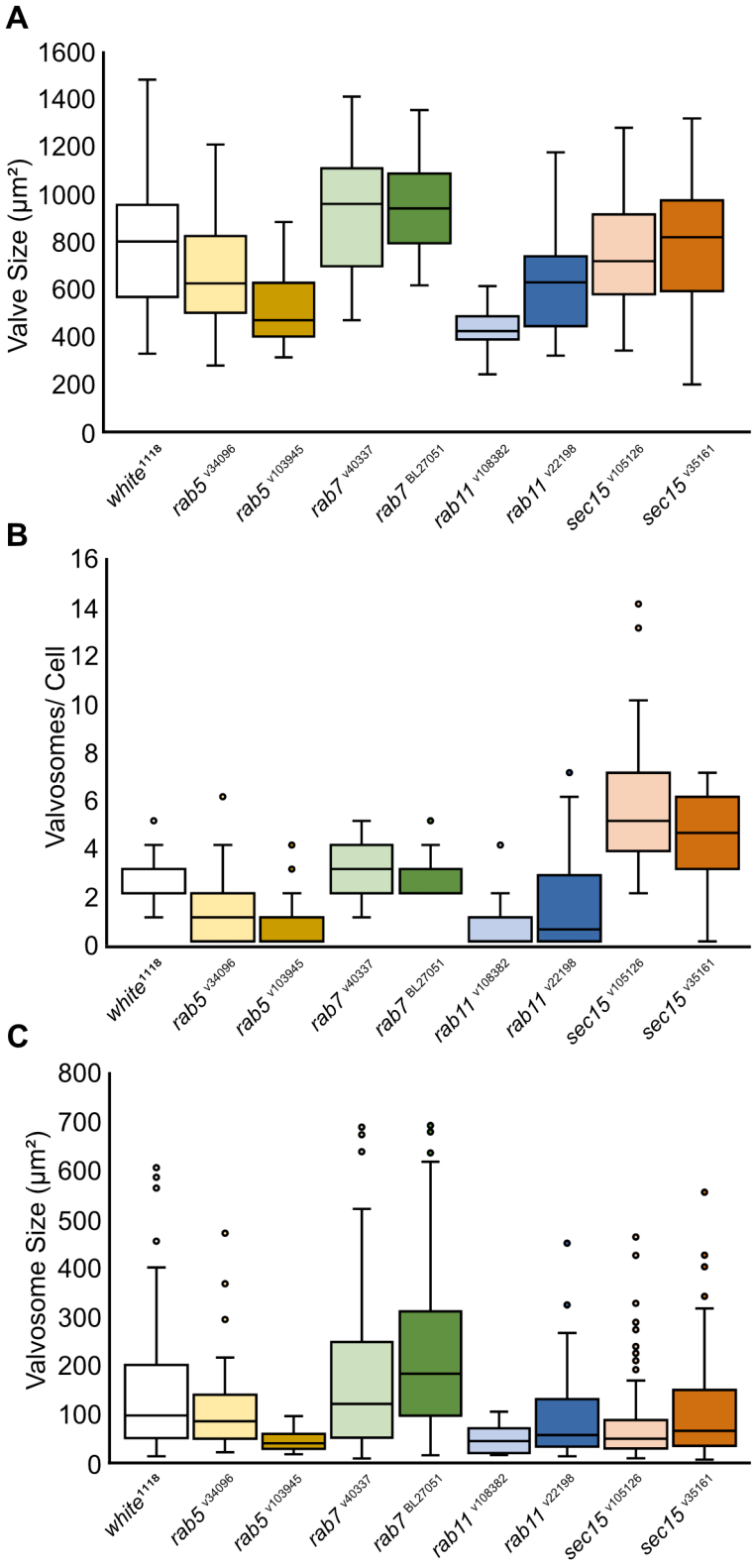

Fig. S2. Effect of heart specific knockdown of different Rab GTPases on valve cells. (A) Valve cell size, (B) Number of valvosomes per cell and valvosome size (C). Cells analysed: *white*^{1118} 38 cells, *rab5*^{v34096} 30 cells, *rab5*^{v103945} 40 cells, *rab7*^{v40337} 38 cells, *rab7*^{BL27051} 38 cells, *rab11*^{v108382} 38 cells, *rab11*^{v22198} 40 cells, *sec15*^{v105126} 38 cells, *sec15*^{v35161} 30 cells. All RNAi lines were driven by *hand*C-GFP; *hand*C-Gal4 line.

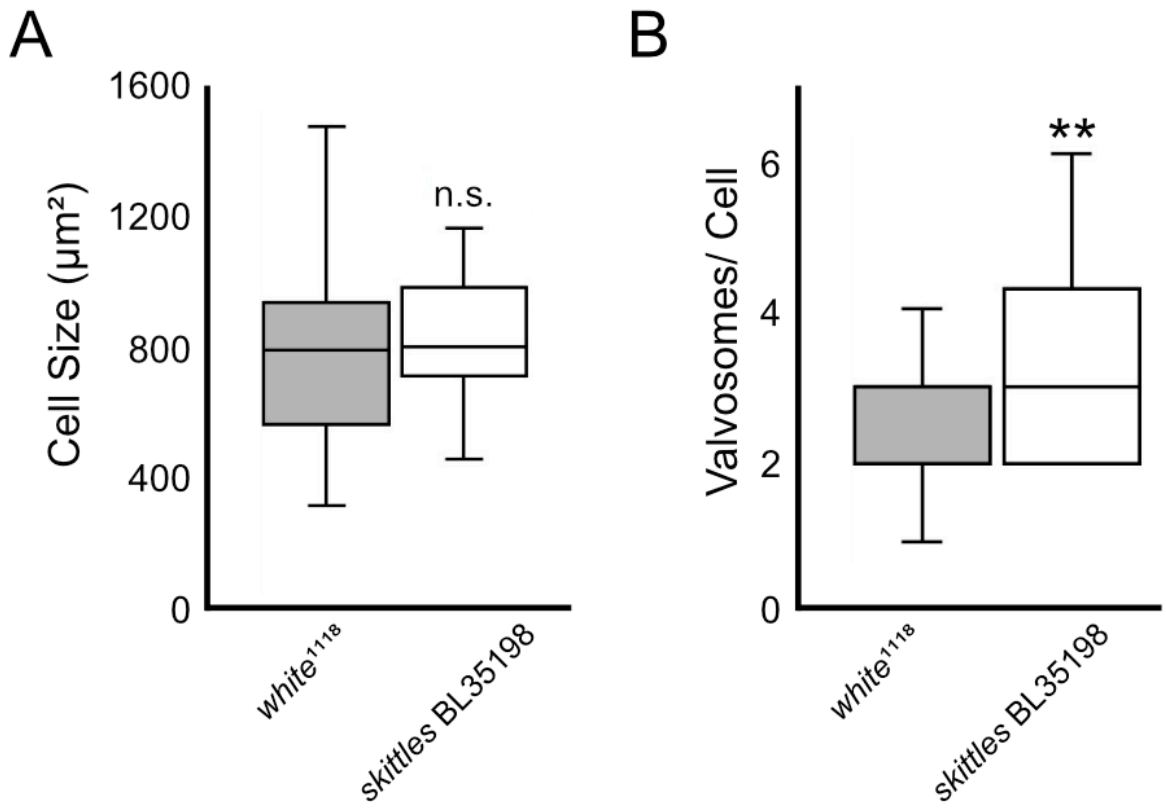

Fig. S3. Heart specific downregulation of *skittles*. Depletion of the PIP5 kinase skittles, has no effect on cell size (A) but leads to an increased number of valvosomes per cell (B). Cells analysed: *white*^{1118} = 38 cells, *skittles* (BL35198) = 40 cells (driven by *hand*C-Gal4).

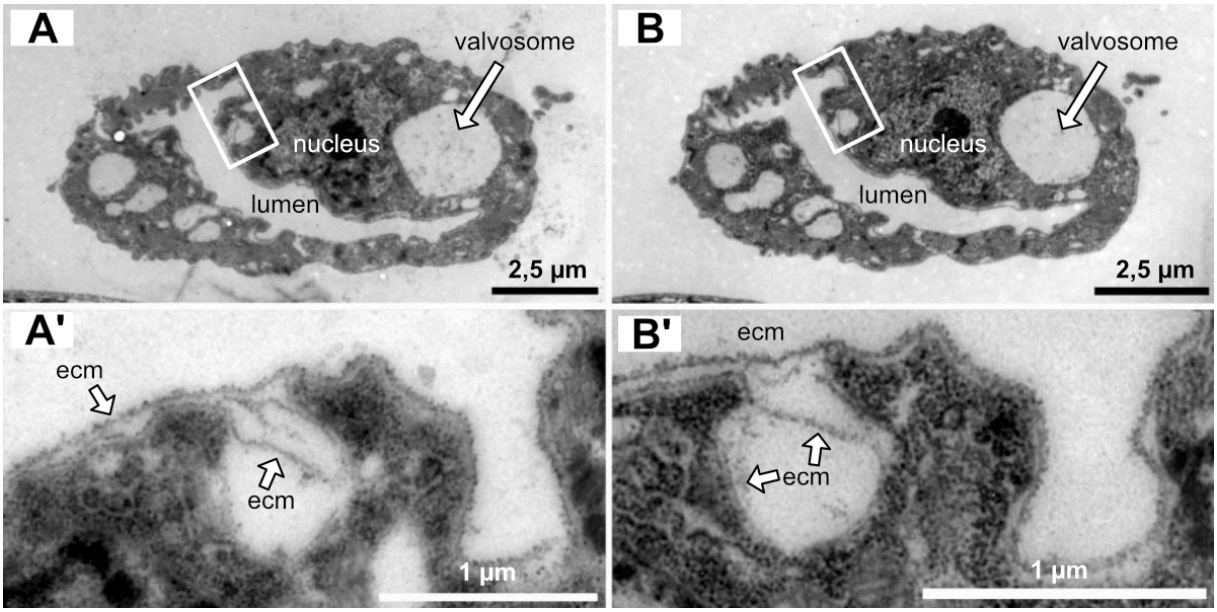

Fig. S4. TEM cross section of 1st instar larva valve cells. (A & B) Overview of larval valve cells with maturing valvosome and plasma membrane invaginations (boxed). (A'-B') Higher magnifications from A & B showing plasma membrane tubulation and presence of ECM on invagination pore.

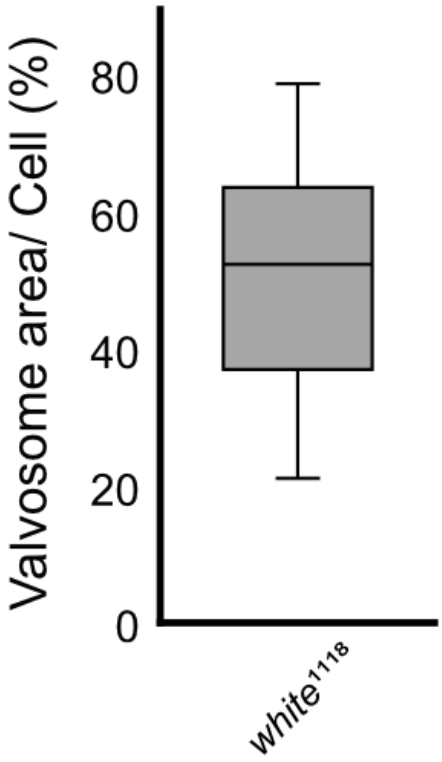

Fig. S5. The valvosomal compartment occupies most of the valve cell area. 40% to 65% of the cells´ area is occupied by the valvosomal compartment. Cells analysed *white*^{1118} = 38 cells. Confocal section through the nuclear plane were used.

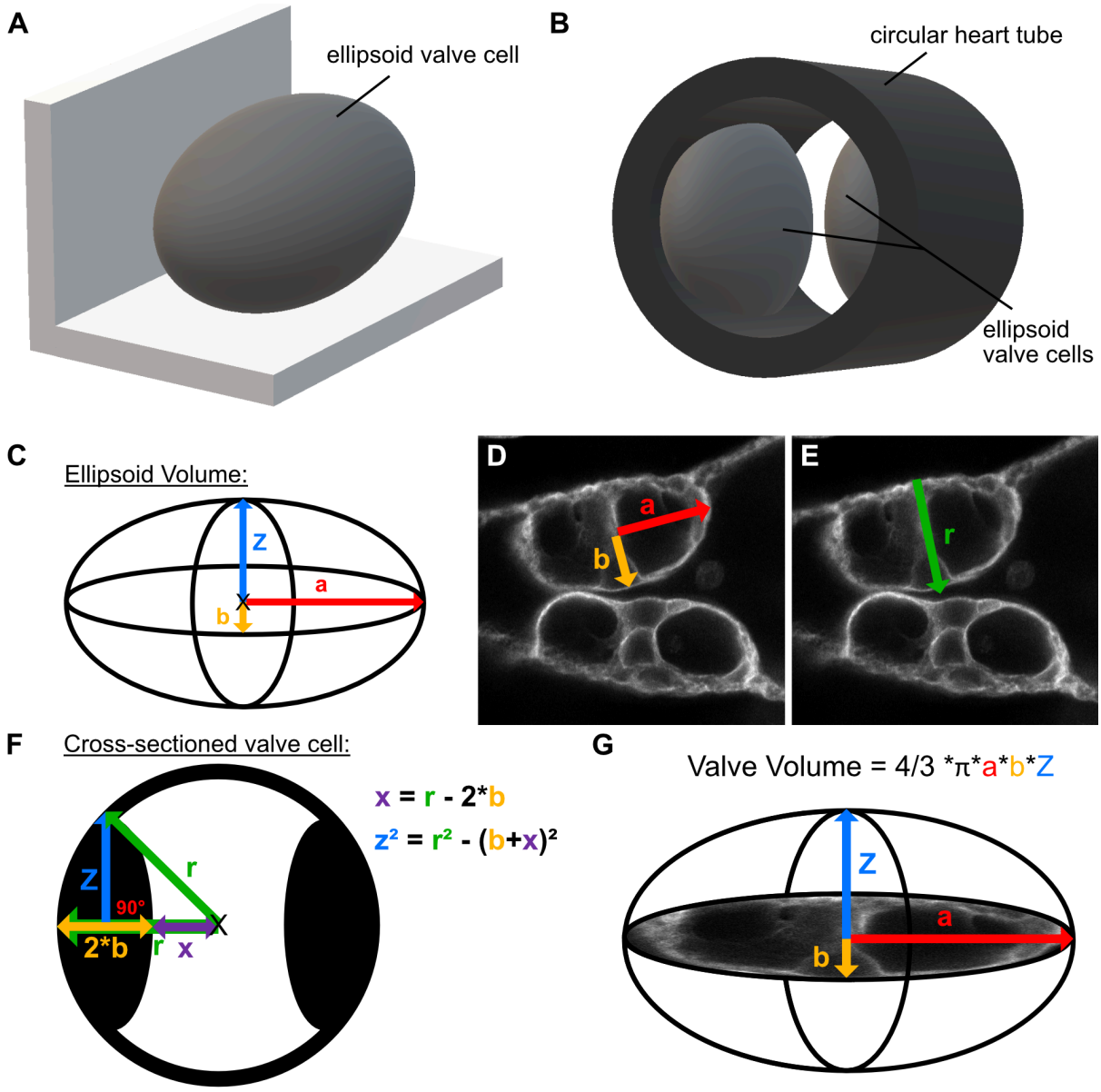

Fig. S6. Calculation of valve cells volume from confocal live recordings of intact 3rd instar larva. Volume calculation is possible assuming an ellipsoid shape of the valve cell (A) and a circular heart tube (B). For valve cell volume calculation three factors (*a*, *b* & *Z* in C) have to be determined. (D & E) Scheme illustrating points of measurements. Factors a and b were determined as half of the width/ length of the valve cell respectively and radius r as half of the total heart tube diameter at the position of the valve cells. (F) Applying the theorem of Pythagoras, the depth of the cell, factor Z, is determined. The three factors a, b, and Z were determined for the cell in the closed and in the open state and volume was calculated with the given formular (G).

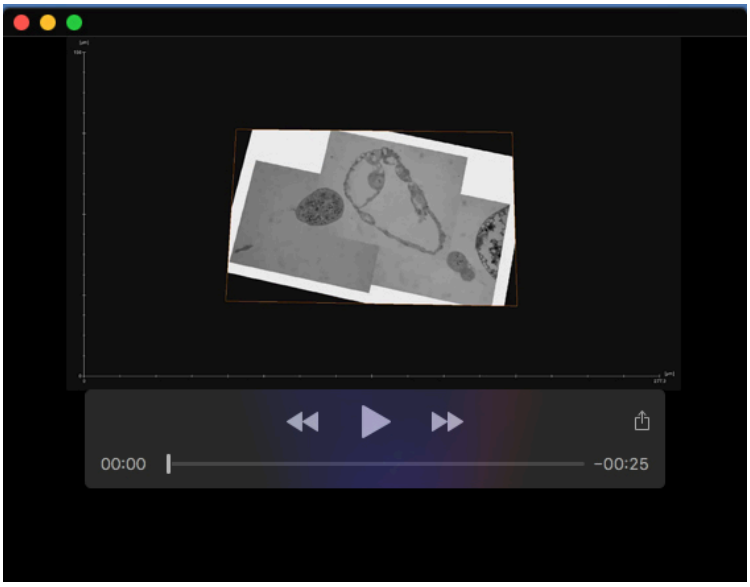

Movie 1. 3D reconstruction of valve cells and valvosome from 700nm semi-thin sections.

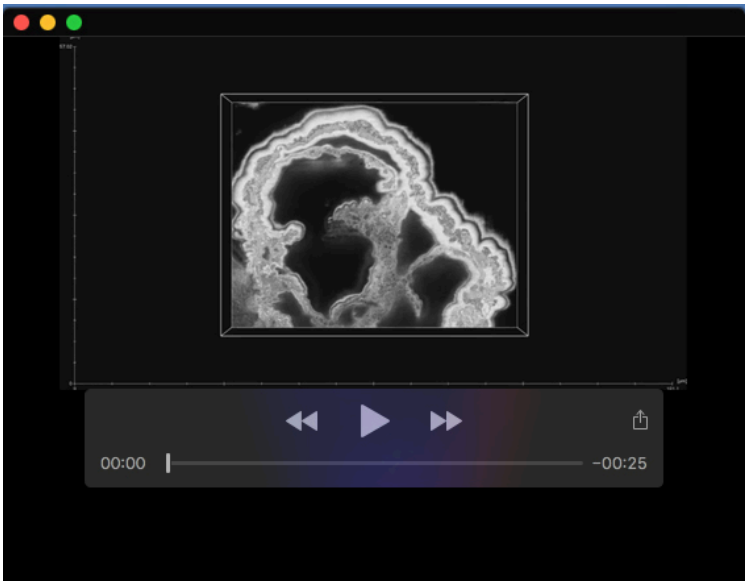

Movie 2. Serial Block Face analysis of valve cells and 3D reconstruction reveals connections between valvosomes.

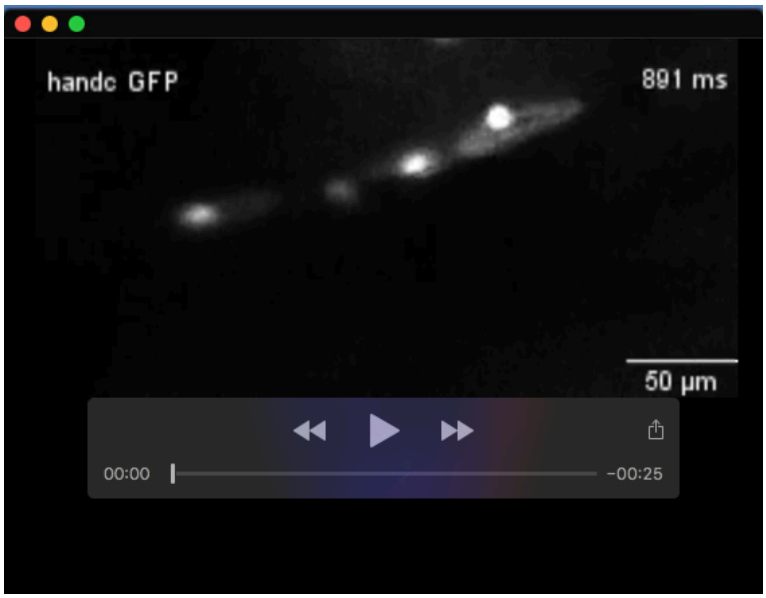

Movie 3. Slow motion video (6fps) of intact *Drosophila* larva valve cells utilising a *hand*C-GFP reporter line captured for 10 sec at ~81ms/ frame (12 fps).

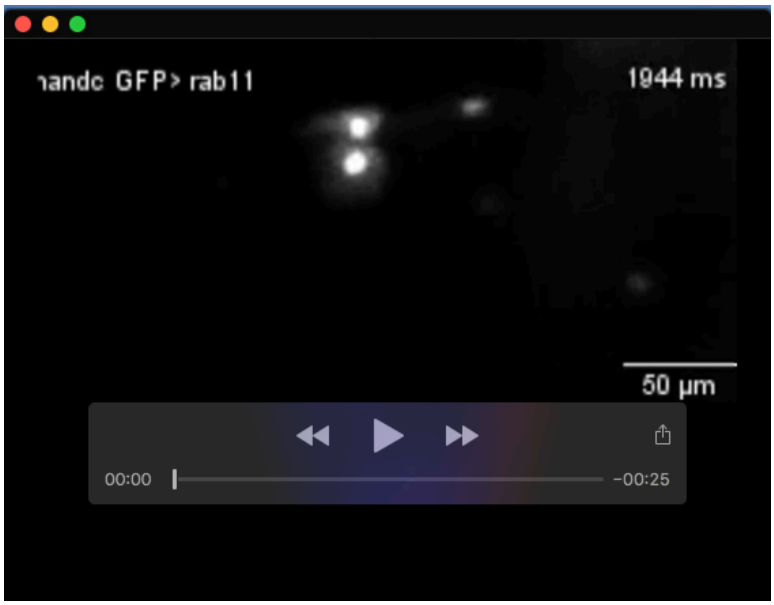

Movie 4. Slow motion video (6fps) of intact *Drosophila* larva valve cells utilising a *hand*C-GFP reporter *hand*C-Gal4 line driving RNAi of *rab11*, captured for 10 sec at ~81ms/ frame (12 fps).